

The Geological Society of America  
Special Paper 436  
2008

## ***Sediment waves in the Bismarck Volcanic Arc, Papua New Guinea***

**Gary Hoffmann**

**Eli Silver**

**Simon Day**

**Eugene Morgan**

*Earth Sciences Department, University of California, Santa Cruz, California 95064, USA*

**Neal Driscoll**

*Scripps Institution of Oceanography, La Jolla, California 92093, USA*

**Daniel Orange\***

*AOA Geophysics, Castroville, California 95012, USA*

### **ABSTRACT**

In the Bismarck Volcanic Arc in Papua New Guinea, six fields of sediment waves were imaged with sonar. Sediment structures observed in seismic data and swath bathymetry are not unique and can result from predominantly continuous (bottom) currents, or episodic (turbidity) currents, or from deformation of sediment. Two of these wave fields overlap and appear to be of turbidity-current origin and modified by bottom currents, with one field unconformably overlying the other field. A field off the coast of Dakataua caldera displays an arcuate morphology, and a series of enclosed depressions within the field suggests creation by extensional deformation of rapidly deposited sediment. Scour features in side-scan imagery suggest turbidity-current activity, which also likely modifies the sediment waves. The wave field is isolated from hyperpycnal currents, however, suggesting that in the absence of a shelf, coastal erosion and small landslides can produce semiregular gravity-driven sediment flows that deposit in deep (>1400 m) water. In Kimbe Bay a fourth sediment-wave field also displays arcuate morphology and enclosed depressions within the field. This wave field is found within a bay >40 km from shore and also appears to have been formed by a combination of extensional deformation of sediment and energetic current activity. Two additional fields in Hixon Bay are fed by small and medium rivers (<~450 m<sup>3</sup>/s mean annual discharge) draining volcanoes and mountainous regions. One small field appears within a slide scar, suggesting that the initial topography of the scar provided the conditions for early sediment-wave growth. A much larger field is best explained by repeated hyperpycnal currents originating from the Pandi River. We cored a series of upward-fining, graded sequences consistent with a turbidity-current origin. Ages from these cores and measurements of relative thickness in sub-bottom imagery of the

---

\*Present address: Black Gold Energy, Plaza Kemang Timor 22, Jakarta 12510, Indonesia

Hoffmann, G., Silver, E., Day, S., Morgan, E., Driscoll, N., and Orange, D., 2008, Sediment waves in the Bismarck Volcanic Arc, Papua New Guinea, in Draut, A.E., Clift, P.D., and Scholl, D.W., eds., Formation and Applications of the Sedimentary Record in Arc Collision Zones: Geological Society of America Special Paper 436, p. 91–126, doi: 10.1130/2008.2436(05). For permission to copy, contact editing@geosociety.org. ©2008 The Geological Society of America. All rights reserved.

**field constrain deposition rates for the field and suggest that a large part of the Pandi River discharge must be bypassing the shelf and depositing on the sediment-wave field in deep water (>1200 m). These findings suggest that the sedimentary record in arc collision zones will be dominated by mass-wasting deposits very close to volcanoes, and by river discharge depositing in select, extent regions far from shore. Because sedimentation rates can vary by a factor of 2 between the two flanks of a sediment wave, care must be taken when comparing bed thickness across an entire sedimentary section.**

**Keywords:** sediment waves, Papua New Guinea, Bismarck Sea, marine geology, geomorphology.

## INTRODUCTION

More than half of the total suspended sediment supplied by rivers to the sea originates from small to medium mountain rivers (<~450 m<sup>3</sup>/s mean annual discharge; Mulder et al., 2003), especially those in tectonically active regions such as the Bismarck Volcanic Arc in Papua New Guinea (Milliman and Syvitski, 1992). At another active arc-continent collision, Taiwan, as much as 42% of the sediment discharge to the ocean occurs by hyperpycnal flows (>40 g/L; Warrick and Milliman, 2003), typically during flood events (Dadson et al., 2005). Large earthquakes can cause an increase in the occurrence of hyperpycnal flows and the percentage of sediment discharged at hyperpycnal concentrations for some rivers for short intervals, owing to landslides (Warrick and Milliman, 2003; Dadson et al., 2005). Under certain conditions, these hyperpycnal turbidity currents can result in deep-sea sediment waves (H.J. Lee et al., 2002; Wynn and Stow, 2002; Schwehr et al., 2007).

The Bismarck Volcanic Arc differs from arc-collisional settings such as Taiwan and other regions where turbidity-current sediment waves have been identified (for example, the Var field southeast of France; Migeon et al., 2001) by having active volcanism. Widely dispersed tephra may increase the frequency of hyperpycnal discharges (Hayes et al., 2002), and ashfall from volcanic eruptions may also directly produce turbidity currents (Fiske et al., 1998). Bottom currents, rapid slope failure, and slow soft-sediment deformation, for instance caused by repeated earthquake loading, are also processes that have been suggested as being capable of producing or greatly modifying sediment-wave fields (Gardner et al., 1999; Lee and Chough, 2001; H.J. Lee et al., 2002; Wynn and Stow, 2002). O'Leary and Laine (1996), H.J. Lee et al. (2002), and Wynn and Stow (2002) provide criteria to distinguish among these various processes.

Because large undulations (hundreds of meters to a few kilometers) are easily identifiable in sonar surveys of the seafloor, and hyperpycnal turbidity currents are greatly affected by climate, uplift, and seismicity (Mulder et al., 2003), turbidity-current-generated sediment-wave fields should be ideal targets for studying these factors in arc and arc-collisional environments. In the Bismarck Sea we imaged multiple sets of large sediment waves,

giving us the rare opportunity to examine the distinguishing criteria using multiple wave fields within the same data set. We can also test if these criteria can be consistently applied to differentiate wave-forming processes, and what sediment waves formed by these processes tell us about dispersal of sediment.

We begin with a discussion of the processes that create sediment waves and morphologically similar features. One of these processes, turbidity currents, is surrounded by some controversy, and so we proceed with an examination of the term and its relation to hyperpycnal currents. We follow the discussion of sediment-wave-generation processes and turbidity currents with our specific observations and discuss them in terms of their distinguishing features and how they relate to climate and sediment transport in the Bismarck Sea.

## STUDY LOCATION

Papua New Guinea has two seasons, the summer monsoon season and the winter trade-wind season. Although cyclonic events are uncommon, near-continuous tropical rain produces frequent landslides and consequent large sediment discharge to the coastal ocean from the mountains, as well as by floods any time of year (McAlpine and Keig, 1983; Pickup, 1984; Walsh and Nittrouer, 2003). The sediment load for the entire island of New Guinea is high, at ~1.7 × 10<sup>9</sup> t yr<sup>-1</sup>, roughly the estimated load of all North American rivers combined (Milliman, 1995).

The Bismarck Volcanic Arc is located in northern Papua New Guinea and forms the southern boundary of the Bismarck Sea (Fig. 1). In the eastern half of the arc the Solomon Sea plate is subducting beneath the Bismarck Sea plate at the New Britain Trench (Johnson, 1979; Taylor, 1979). In the west, subduction has ceased as the Finisterre and Adelbert terranes, parts of a remnant Paleogene volcanic arc that lies in the Bismarck forearc, collide with the Australian plate and are being uplifted to form the Finisterre and Adelbert Mountains (Abbott et al., 1994; Pigram and Davies, 1987).

The volcanism in the arc is related to subduction of the Solomon Sea plate and occurs behind the remnant Paleogene arc, which also includes the island of New Britain. The submarine environment surrounding the Bismarck Volcanic Arc was

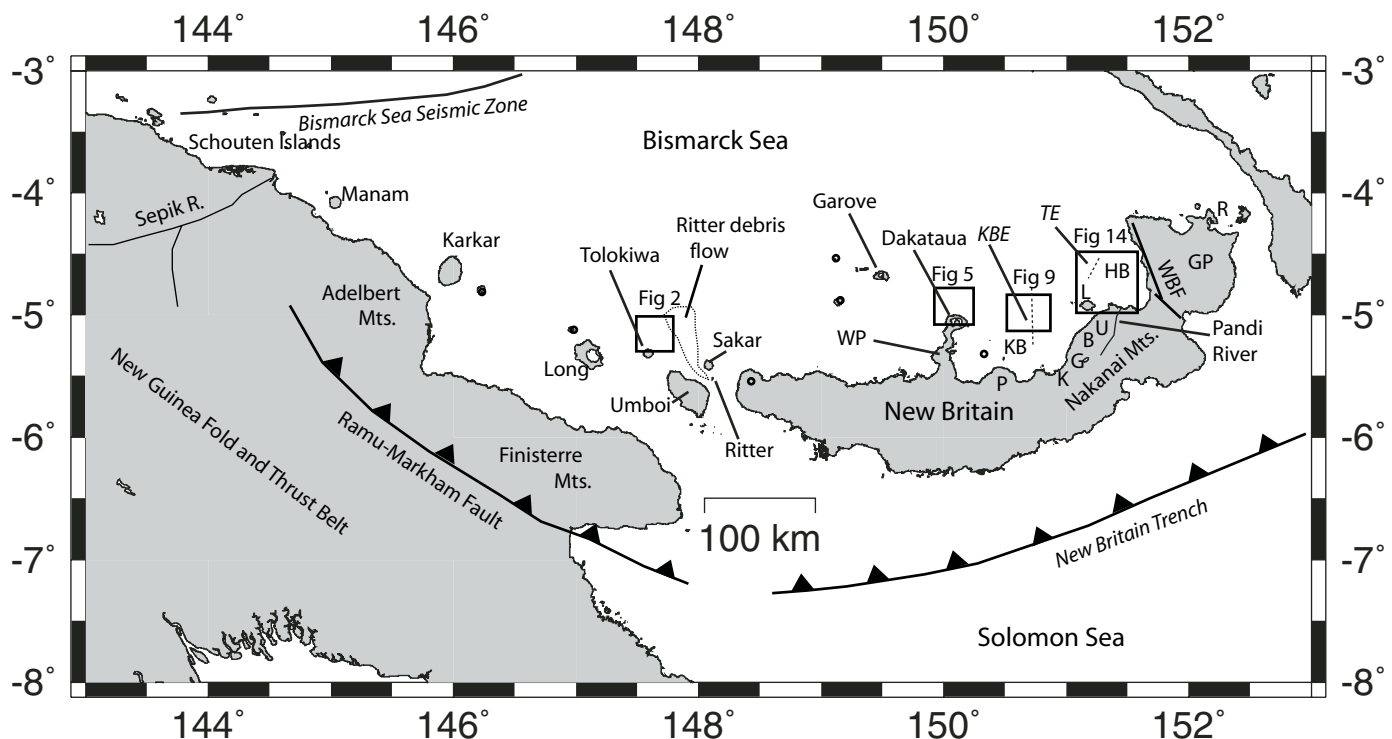


Figure 1. Location map showing regional setting of the wave fields of the Bismarck Volcanic Arc. The New Britain Trench accommodates subduction of the Solomon Sea plate. New Britain and the Finisterre and Adelbert terranes are parts of a remnant Paleogene arc. The modern subduction-related volcanic arc is offset to the north of the remnant arc. From west to east, some of the modern volcanoes include the Schouten Islands, Manam, Karkar, Long, Tolokiwa, Umboi, Sakar, Ritter, Garove, Dakataua and the Willaumez Peninsula (WP), Pago (P), Karai (K), Gallosfculo (G), Bamus (B), Lolobau (L), Ulawun (U), and Rabaul (R), which lies on the northeast tip of the Gazelle Peninsula (GP) on the island of New Britain. The Willaumez Peninsula is composed of a north-south string of volcanoes. The locations of several other volcanoes are shown as small black circles. Major faults in the region include the Ramu-Markham Fault and the Wide Bay Fault (WBF). Two new faults were mapped during this survey: the Kimbe Bay Escarpment (KBE) in Kimbe Bay (KB), east of the Willaumez Peninsula, and the Torkoro Escarpment (TE), in the Hixon Bay region (HB) north of Lolobau. The outline of the debris flow from the 1888 collapse of Ritter Island is shown. The Sepik River is the largest river on the north coast of Papua New Guinea. It drains a large part of the New Guinea Fold and Thrust Belt. The Pandi River drains a large part of the Nakanai Mountains in New Britain, and the eastern flanks of Ulawun and Bamus volcanoes. The locations of Figures 2, 5, 9, and 14 are shown.

the target of this study. We mapped submarine volcanic collapse features, including deposits of the 1888 Ritter Island collapse (Johnson, 1987), for input into tsunami models (e.g., Ward, 2001). The locations of a selection of volcanoes in the arc are shown in Figure 1. The arc extends westward to the Schouten Islands between 143°E and 145°E, where it meets the Bismarck Sea seismic zone. It extends east to ~152°E at Rabaul caldera on the northeast tip of the Gazelle Peninsula. The study area includes the Schouten Islands in the west but goes only so far as the Hixon Bay area just west of the Gazelle Peninsula. The Gazelle Peninsula is moving northwest relative to the rest of the island of New Britain along the left-lateral Wide Bay Fault (Fig. 1; Madsen and Lindley, 1994). The Wide Bay Fault defines the eastern edge of the Hixon Bay region, where we mapped a new fault, the Torkoro Escarpment.

The study area includes the deep-water (>500 m depth) environment around the volcanoes in the arc, including on either side of the Willaumez Peninsula, a string of volcanoes

that juts northward from New Britain into the Bismarck Sea, ending in Dakataua caldera. To the east of the Willaumez Peninsula is Kimbe Bay, which is bounded on three sides by large volcanoes. It is also the location of a newly mapped fault, the Kimbe Bay Escarpment.

Collapse blocks were found near several volcanoes during the survey, including off Tolokiwa Island and off Dakataua caldera. At both these locations, sediment-wave fields were also mapped nearby. Sediment-wave fields were also mapped in Kimbe Bay and the Hixon Bay region (boxed regions of Fig. 1). These sediment-wave fields form the basis of the current paper.

## SEDIMENT-WAVE FORMATION AND DISTINCTIVE FEATURES

*Sediment waves*, in the most common use of the term, refers to any undulating pattern that is caused by differential sediment deposition and erosion over time, analogous to dunes or antidunes,

as opposed to undulating patterns that are caused by slope failure such as slow deformation or slide events (H.J. Lee et al., 2002; Wynn and Stow, 2002). Large undulations with wavelengths of 100 m to >10 km are observed in a variety of settings, including on channel levees, axes, and mouths or in canyons (Normark et al., 1980; Kidd et al., 1998; Nakajima and Satoh, 2001; Migeon et al., 2001; Lewis and Pantin, 2002); on the flanks of volcanic islands (Wynn et al., 2000); in troughs (Howe, 1996); and on plateaus and continental slopes (Lee and Chough, 2001; O'Leary and Laine, 1996). Short-wavelength (0.1–1 m) sediment waves have been observed in settings such as terrestrial rivers (Mohrig and Smith, 1996; Jerolmack and Mohrig, 2005a, 2005b; Coleman et al., 2005). Owing to imaging limitations in the deep-sea environment, however, we confine our current discussion to large sediment waves.

Two processes are recognized as producing sediment waves as defined here, namely turbidity currents and bottom currents (Wynn and Stow, 2002; Schwehr et al., 2007). Waves of turbidity-current origin are created by numerous episodic events preferentially depositing sediment on the upstream flank of the waves in antidiad fashion when the flow is in the Froude number regime of ~0.5–1.9 (Hand, 1974; Bowen et al., 1984; Wynn et al., 2000; H.J. Lee et al., 2002). The Froude number is the ratio between current speed and the speed of gravity waves in a density-stratified fluid, such as a sediment-laden-current layer in seawater. Recent research suggests that initiation of a turbidity-current sediment-wave field may require breaks in slope or preexisting undulations, but once started, these wave fields may grow on their own (Ercilla et al., 2002; H.J. Lee et al., 2002; Kubo and Nakajima, 2002).

Deep-sea sediment waves caused by turbidity currents generally have wavelengths of 200 m to 7 km, and wave heights of 2–70 m, and occur on slopes ranging from 0.1° to 0.7° (Wynn and Stow, 2002; H.J. Lee et al., 2002). In profile, the waves migrate upstream and upslope because of preferential deposition on the upstream flank (Wynn and Stow, 2002; H.J. Lee et al., 2002). Internal reflections are commonly continuous between waves (H.J. Lee et al., 2002). Wave crests tend to be oriented perpendicular to the local slope, as turbidity currents travel downslope (Wynn and Stow, 2002; H.J. Lee et al., 2002; Schwehr et al., 2007). Wave sequences progressively thin downslope, wave heights can decrease downslope, and some reflections pinch out downslope in profile, since sediment concentration and deposition in turbidity currents progressively decrease downslope (Mulder et al., 1998). Thus deposition in the distal end will be from large events that occur only rarely (H.J. Lee et al., 2002). Wave crests tend to be linear or sinuous in plan view, with some bifurcation (Wynn and Stow, 2002; H.J. Lee et al., 2002). Waves formed by turbidity currents are often associated with other evidence of turbidity-current activity, such as channels, levees, and scour features. In their review, H.J. Lee et al. (2002) note that the overall cross-sectional shape of a sediment-wave field is commonly concave upward.

The generally accepted concept of bottom-current sediment-wave generation is that internal waves induced within a current in a density-stratified medium flowing over topography will differentially deposit and erode sediment on the seafloor (Flood, 1988). Sediment waves formed by bottom currents have similar dimensions as turbidity-current-generated waves (Wynn and Stow, 2002). Wave crests tend to be linear or sinuous with bifurcations (Wynn and Stow, 2002). Bedforms often migrate upcurrent but can also migrate downcurrent (Wynn and Stow, 2002). They are distinct from turbidity-current-generated sediment waves in that they can form on very low slopes or flat seafloor, and wave crests are often aligned obliquely to the slope because the currents are contour-parallel (Wynn and Stow, 2002). Both bottom- and turbidity-current-generated waves tend to display asymmetry between flanks in backscatter imagery (H.J. Lee et al., 2002).

Undulating patterns can also arise from deformation, however. These can occur from extension (O'Leary and Laine, 1996) or compression (Lee and Chough, 2001; Hill et al., 2004). These undulating patterns may be related to rapid slope failure, such as slumps (H.J. Lee et al., 2002), or to slow deformation caused by intermittent earthquake loading (Lee and Chough, 2001). These features can be up to 10 km in wavelength, and up to 100 m in wave height (Wynn and Stow, 2002), and they can occur on steep slopes or very shallow slopes (<0.5°; Lee and Chough, 2001). In profile, deformational features are commonly associated with faulting (O'Leary and Laine, 1996; H.J. Lee et al., 2002). Plan-form imagery of these features is rare, but wave crests may be arcuate, without bifurcation (Wynn and Stow, 2002).

Bottom currents, turbidity currents, and deformation can all interact in the creation of sediment-wave fields (Howe, 1996; Faugères et al., 2002; H.J. Lee et al., 2002). In this manuscript we will try to tease out the dominant and subordinate processes responsible for creating these morphologic “sediment-wave” features.

## TURBIDITY FLOWS AND HYPERPYCNAL CURRENTS

Considerable controversy exists regarding the nature of flow and deposits of turbidity currents, as well as the terms used in the literature that apply to various sediment transport regimes (Kneller and Buckee, 2000; Shanmugam, 2000; Mulder and Alexander, 2001; Mulder et al., 2001; Shanmugam, 2002; Mulder et al., 2002). For the sake of clarity in our present discussion, we note an overlap between the terms *hyperpycnal current* and *turbidity flow*, and we define our particular usage in this paper.

Following Mulder and Alexander (2001), *hyperpycnal current* refers to sediment-laden river discharge that is denser than the body of water into which it enters. The flow can travel long distances in a semidiscrete layer, entraining fluid and possibly additional sediment if it is exerting shear stresses on the bed high enough to cause erosion (Skene et al., 1997; Mulder and

Alexander, 2001; Mulder et al., 2003). For river discharge entering seawater, the sediment concentration needs to be at least  $\sim 40 \text{ kg m}^{-3}$  for the flow to be negatively buoyant (Mulder and Syvitski, 1995; Warrick and Milliman, 2003). Depending on the river, hyperpycnal-discharge events can occur about once every 100 yr, or as often as once per year (Mulder et al., 2003).

*Turbidity flow* refers to sediment suspended primarily by the upward component of turbulence (Lowe, 1982; Middleton, 1993; Stow et al., 1996; Shanmugam, 2000; Mulder and Alexander, 2001). Such flows contain suspended sediment concentrations up to 10% by volume (Shanmugam, 2000; Mulder and Alexander, 2001). They can be generated by a number of mechanisms, such as entrainment of sediment into surrounding seawater at the upper surface of a debris flow. Other mechanisms include hyperpycnal river discharge, and concentration processes in a low-density layer (Lowe, 1982; Middleton and Hampton, 1976; Parsons et al., 2001) such as a layer of tephra fallout during eruptions (Fiske et al., 1998). Coastal erosion during storm events that affect easily eroded sequences could also generate turbidity currents (Hayes et al., 2002). Scully et al. (2002), for instance, showed that energetic water waves increase the capacity for critically stratified gravity flows to transport sediment. Combined with direct turbidity-current generation from ashfall and indirect formation from reworking of tephra, the presence of volcanoes may significantly increase the occurrence of turbidity-current generation in this setting over other settings. We will therefore use *turbidity current* to refer to a sustained turbidity flow generated by any mechanism, and *hyperpycnal current* to refer to turbidity currents generated owing to hyperpycnal discharge at river mouths.

## METHODS

Multibeam bathymetric data were collected aboard the R/V *Kilo Moana* on cruise KM0419, using a hull-mounted SIMRAD EM-120 echo sounder. Backscatter data were collected using a towed MR1 side-scan sonar system. Side-scan data were gridded in a 16 m grid. Multibeam bathymetry and backscatter data were collected along the 1000 km length of the arc in a swath up to 100 km wide. Bathymetric data were median filtered, using a 500 m kernel. High-resolution Compressed High Intensity “Radar” Pulse (CHIRP) sub-bottom sonar data were collected with an Edgetech 1–6 kHz swept frequency with a 50 ms duration. The CHIRP data are unmigrated. This system transmitted approximately every 5–10 m along selected transects. Penetration was up to a few tens of meters. Twelve short ( $<2 \text{ m}$ ) gravity and piston cores were collected, primarily targeting volcanic-collapse debris flows identified in side-scan imagery.

We examine four sediment-wave fields that were identified in the Bismarck Arc in order to determine the various generation mechanisms of the sediment-wave fields. Doing so will help us understand how material is transported through the arc system and how important slope failure is compared to bottom and

turbidity currents. We begin in the central part of the arc north of Tolokiwa, and then continue eastward to look at Dakataua, Kimbe Bay, and Hixon Bay (Fig. 1).

## TOLOKIWA WAVE FIELDS

Tolokiwa Island volcano, near the center of the Bismarck Volcanic Arc (Fig. 1), has undergone at least one lateral collapse in the Holocene. The sediment waves occur in a field north of the island on the northern side of a broad channel ~8 km wide and 40 m deep that grades at  $\sim 0.2^\circ$  to  $0.5^\circ$  from west to east into the basin (Fig. 2).

Two sediment-wave fields overlap in this region. The first is composed of large sediment waves with wavelengths of 600 m to 1 km and wave heights of  $\sim 10 \text{ m}$  to 40 m (Fig. 3). The second field is composed of smaller sediment waves with wavelengths of 100 m to 400 m and wave heights of a few meters (Fig. 3; Fig. 4C, E). Waves in both sets are identifiable in side-scan images as having a distinctly higher backscatter along the eastern flanks (Fig. 3).

The field of large sediment waves is overlapped by the field of small sediment waves, with some small waves appearing between and overlying large waves (Fig. 3; Fig. 4C). The crests of the small waves are oriented slightly oblique to their local slope. This obliquity varies from wave to wave but is  $<30^\circ$ . The crests of the large waves are perpendicular to the local slope.

The high-backscatter eastern, downslope flanks of the waves correspond to the thinner, more steeply dipping beds of the waves (Fig. 4). The large sediment waves commonly show differential deposition, with the upslope side receiving a factor of 2 or more accumulated sediment than the downslope side. The crests of the sediment waves migrate upslope through time (Fig. 4A, B). The small waves lap onto the large waves (Fig. 4C, D), and they overlie parallel reflectors that begin at a depth of 5 m (Fig. 4E).

## DAKATAUA WAVE FIELD

The Dakataua wave field resides on the northern flank of Dakataua caldera. The field is 24 km by 18 km and elongated N-S (Fig. 5). The average north-dipping slope of the field is  $1.4^\circ$ , with the upslope flanks of the waves dipping south between  $1^\circ$  and  $1.5^\circ$ , and the downslope flanks dipping north  $\sim 10^\circ$ . The wave field as a whole forms a topographic high of up to 200 m relative to the flatter seafloor that surrounds the wave field. The seafloor to the east of the wave field is deeper than that to the west. This difference decreases northward, although north of the 240-m-high ridge at the north end of the field the seafloor maintains an eastward-dipping component of  $\sim 0.15^\circ$  (Fig. 5).

Between the caldera and the wave field, the seafloor dips smoothly at  $\sim 5^\circ$ . In the side-scan data the waves generally do not exhibit asymmetry; however, the downslope flanks nearest the caldera display high backscatter (Fig. 6). Scour features are apparent on the  $5^\circ$  slope leading into the wave field (Fig. 6).

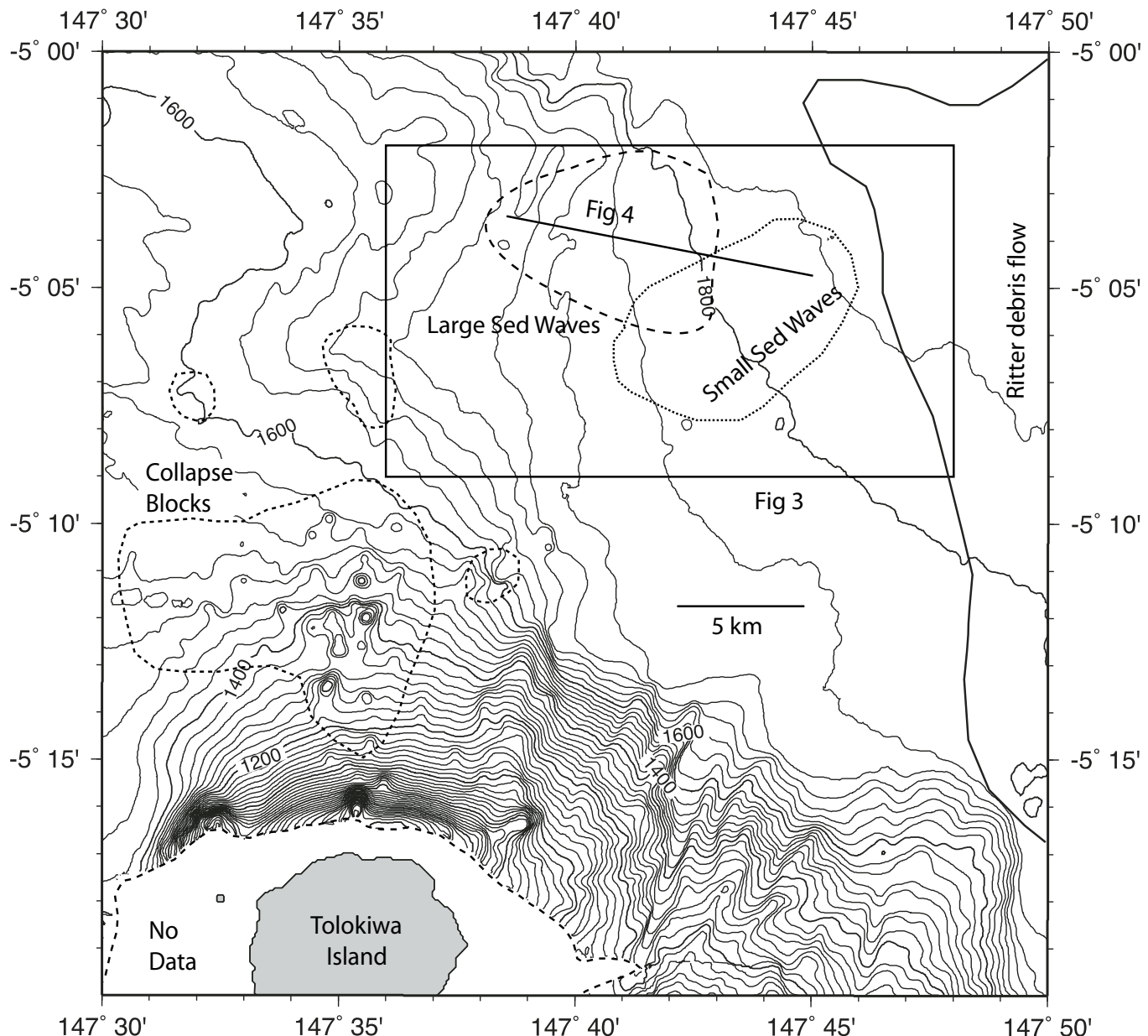


Figure 2. Bathymetry of Tolokiwa sediment-wave fields and surroundings. Two distinct fields overlap—one with wavelengths of 0.6–1 km, labeled large sed waves, and one with wavelengths of 200–400 m, labeled small sed waves. Locations of Figures 3 and 4 are shown. Bathymetric contour interval is 25 m, with annotated contours in bold every 200 m.

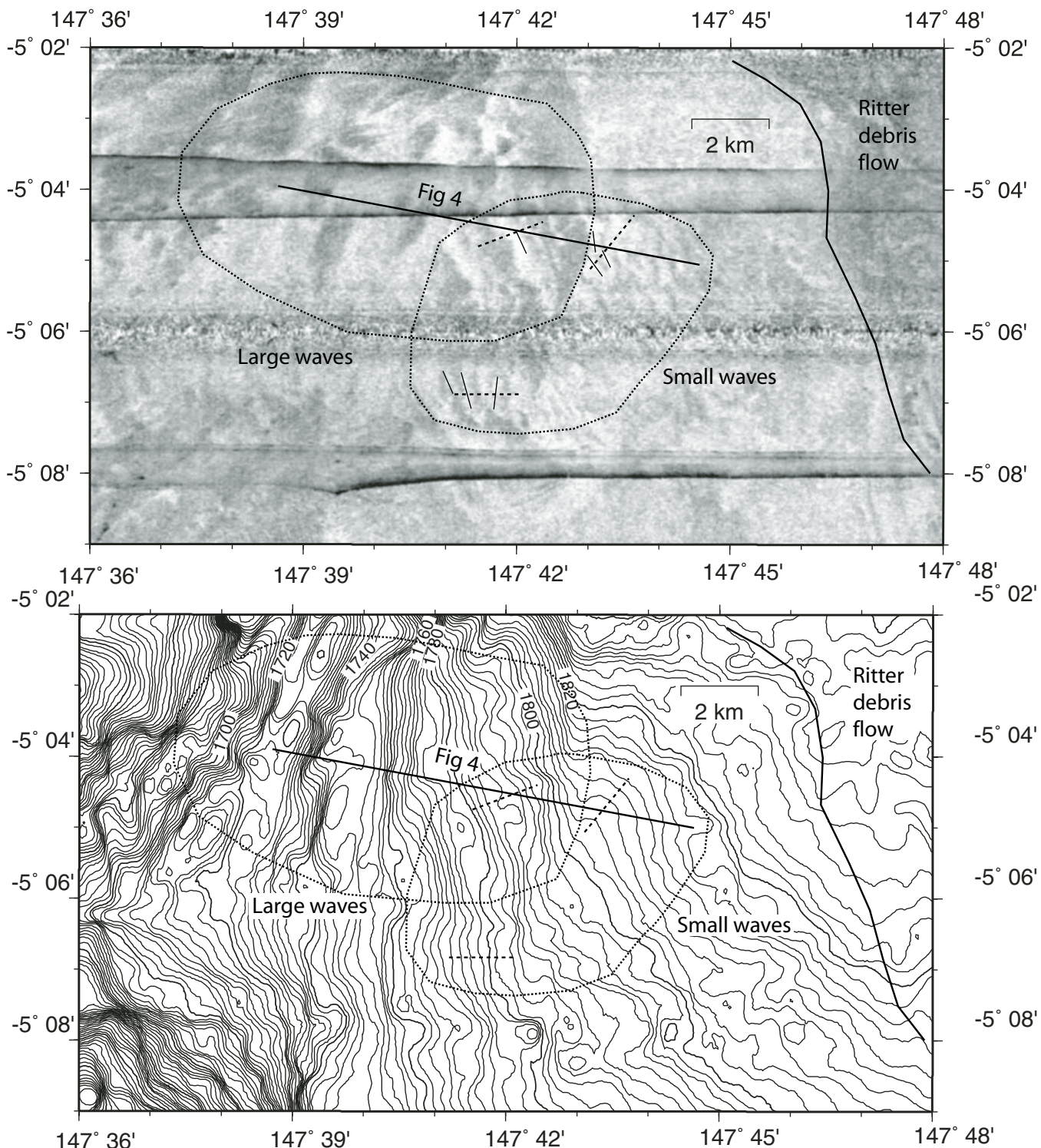


Figure 3. Side-scan mosaic (top) and bathymetry (bottom), contoured at 2 m intervals of Tolokiwa sediment-wave fields. Location of Figure 4 shown. The waves are apparent in the side-scan imagery as features with higher acoustic backscatter (darker shades) in the western flanks than eastern flanks. Insonification direction is north-south. Nadir lines run east-west at 5°02' S and 5°06' S. Black east-west lines are sea-surface reflection artifacts. In both parts of the figure, short dashed lines show local trend of slope. In side-scan image, several wave crests are denoted with short, thin lines to highlight the slight obliquity of the crest-normal to the slope. Dotted lines outline the sediment-wave fields. Note in the side-scan image that some small waves appear within the large waves in the region of overlap.

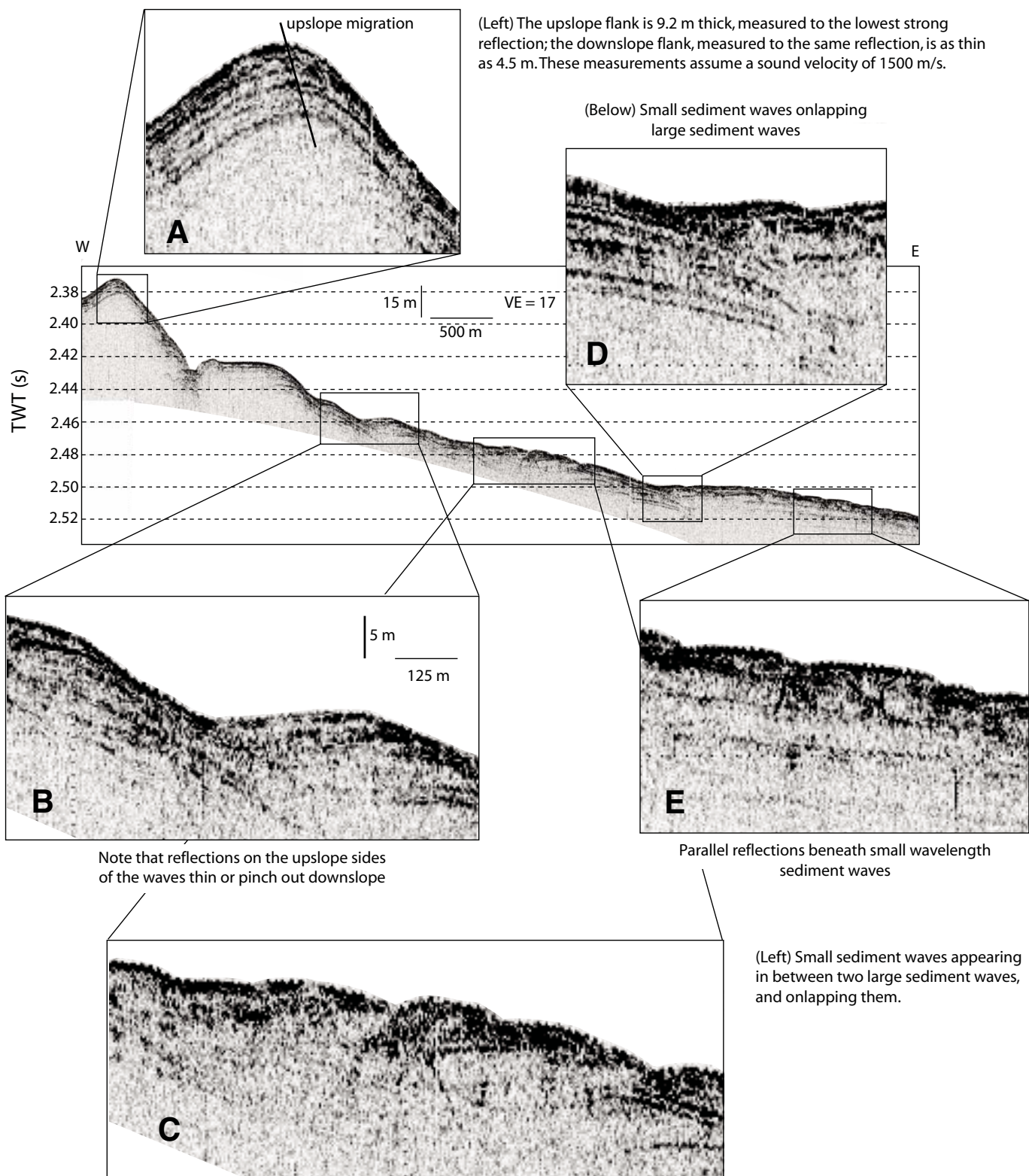


Figure 4. CHIRP profile of eastern end of sediment-wave field north of Tolokiwa Island where the field merges with the ripple field. Location shown in Figure 2. VE—vertical exaggeration; TWT—two-way traveltimes. Enlarged boxes demonstrate particular features of note. All enlarged boxes are at the same scale, which is 4 times larger than and at the same vertical exaggeration as the base figure.

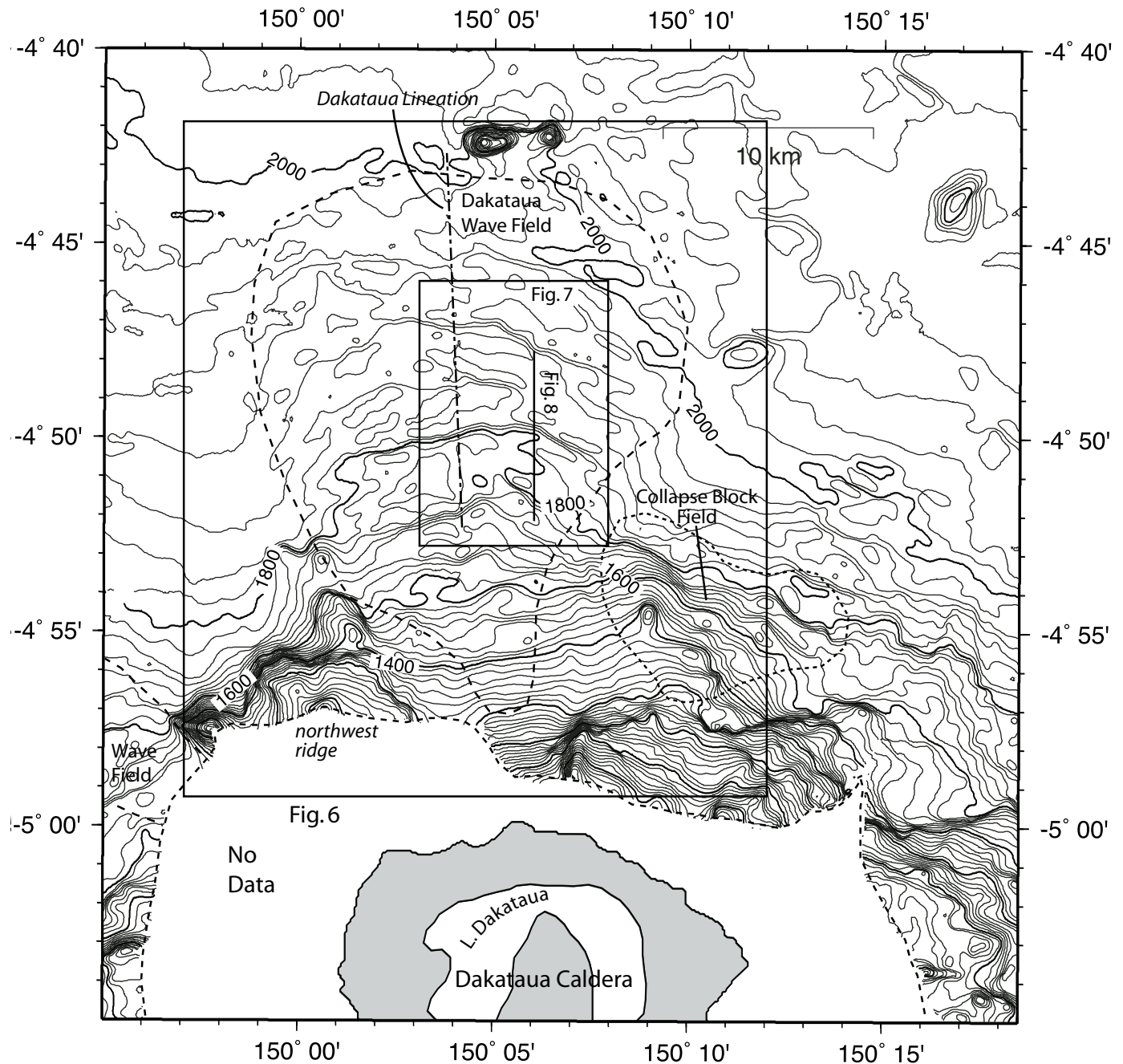


Figure 5. Location map showing wave field in relation to Dakataua caldera and bathymetry (in meters). Contour interval is 25 m, with annotated contours in bold every 200 m. Locations of Figures 6, 7, and 8 are shown. A lineation, shown as the dash-dot line, runs through the field approximately N-S. The lineation ends slightly west of the 240-m-high ridge at the north end of the field.

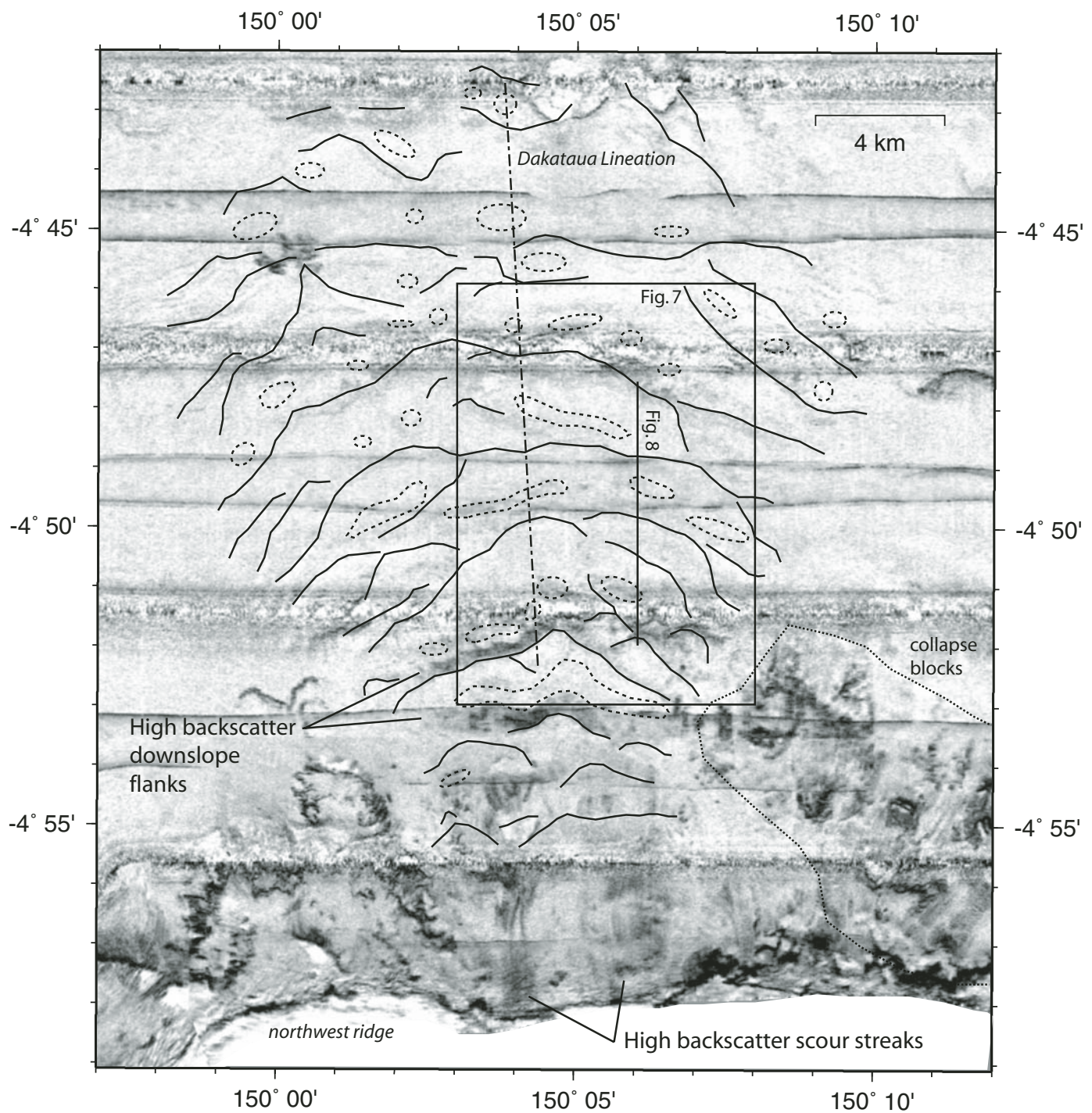


Figure 6. Side-scan mosaic of Dakataua sediment wave field. Locations of Figures 7 and 8 shown. Scale is 1.6 times that of Figure 5. High backscatter is dark. The two elongated regions of high backscatter in the field ( $\sim 4^{\circ}52' S$  and  $4^{\circ}53' S$ ) are in the troughs between waves. Solid lines denote the slope break between wave crests and steep downslope flanks of waves. Dashed lines denote enclosed depressions. The Dakataua lineation is shown as the dash-dot line.

The waves themselves are 1–4 km in length, with wave heights of ~50 m, as measured from the upslope trough to the crest. In plan view they are irregular, although generally arcuate, with crests largely continuous across the width of the field (Fig. 6). The crests are sinuous, and some are bifurcate (Figs. 6 and 7), and they also tend to be wider than the troughs between waves (Fig. 7). Many of the troughs between waves contain enclosed depressions (Figs. 6 and 7). Some of the depressions are associated upslope with steep slopes that display high backscatter, but many are not (Fig. 6), and the depressions are not associated with high backscatter scour.

A lineation runs N-S through the field (Fig. 5), characterized by eastward-dipping slopes, widened depressions, and pinched-out wave crests (Fig. 7). The CHIRP failed to penetrate more than 1 m throughout this field (Fig. 8).

## KIMBE BAY WAVE FIELD

Whereas the Tolokiwa and Dakataua waves are both isolated from large inputs of fluvial sediment, Kimbe Bay is fed on three sides by a multitude of small rivers that drain volcanoes. The Kimbe Bay wave field lies near the center of the bay, almost 50 km from shore, adjacent to the Kimbe Bay Escarpment.

The Kimbe Bay wave field is >30 km long and 15 km wide (Fig. 9). In plan view the waves are generally arcuate, although irregular, with wavelengths varying from 1 to 4 km and wave heights reaching >80 m in some areas (Fig. 9). The average slope of the wave field is 1°. Within the field, many enclosed depressions attain a depth of ~100 m and are found between wave crests (Fig. 10). Some low-wave-height features (~10 m) are found west of the main sediment-wave field. The main wave field lies on a topographic high of up to 250 m relative to the sea floor to the west (Fig. 9). To the east, a crevice ~2 km wide and up to ~100 m deep separates the wave field from the Kimbe Bay Escarpment. To the south of the wave field is a topographic ridge at least 200 m high (Fig. 9). Several channels lead into the crevice between the wave field and the escarpment. One channel is associated with high backscatter as it cuts through the ridge east of the Kimbe Bay Escarpment (Fig. 11), then drops 200 m into a plunge pool (S.E. Lee et al., 2002), which is >100 m deep as measured from the downslope side of the channel (Fig. 9).

The crevice increases in width northward, to nearly 6 km, where depressions appear (Fig. 9). The depressions and the escarpment appear as very high backscatter features in side-scan imagery (Fig. 11). The high backscatter regions within these depressions occur on the southern slopes, and the depressions attain depths up to 75 m (Fig. 12). A lineation is contrasted against the background sediment of the wave field, appearing as a higher backscatter region nearly 10 km long and 1 km wide (Fig. 11).

The steeper, downslope sides of the sediment waves produce higher backscatter than the rest of the wave field (Fig. 11). The slopes of the high backscatter faces of the waves approach

10° (Fig. 10). The high backscatter of the downslope sides of the waves is associated in the CHIRP profiles with thinning sequences and upslope migration (Fig. 13). But in most cases (Fig. 13A, B, D) the upslope migration is apparent only on the steep downslope flanks, and only in a few areas can upslope migration be seen clearly across a whole wave, which might be due to cutting across some waves obliquely (Fig. 13C). Additionally, the character of the reflections varies from wave to wave, especially in terms of penetration depth. Some wave crests are imaged to a depth of ~8 m (Fig. 13B, C), whereas wave crests both upslope and downslope of these crests are imaged only to a depth of 2–3 m (Fig. 13A, D).

## HIXON BAY

Hixon Bay allows us to test whether fluvial sedimentation is an important process far from shore in this system. It is several kilometers wide and the receptacle for the Pandi River (Fig. 14). This river drains ~800 km<sup>2</sup> of the Nakanai Mountains and the eastern flanks of Ulawun and Bamus volcanoes (Fig. 1).

## Backscatter, Morphology, and Sub-bottom Profiles of the Hixon Bay Sediment-Wave Field

A large sediment-wave field is found in the Tokoro Trough of Hixon Bay (Figs. 14–16). This trough attains depths >1900 m, and two channels feed into the trough from the Pandi River (Fig. 14). The sediment-wave field (Fig. 15) begins shortly below the point at which channel scour diminishes between Torkoro and Mele Reefs. A slide scar is present east of Lolobau Ridge and is shown in more detail in Figure 17.

In side-scan images (Fig. 18), high backscatter scour features highlight the Pandi River channels. The slide scar shows a stippled pattern of high backscatter in the upper part, and the edges are highlighted as high backscatter streaks in the lower half of the slide scar. The sediment-wave field (Fig. 18) appears in backscatter as a pattern of alternating higher and lower backscatter, with regions of varying wavelengths. We divide the wave field into six groups on the basis of morphology (Fig. 16), and we summarize their characteristics in Table 1.

The six groups of waves are also distinct from one another in sub-bottom imagery (Table 2). We correlate a transparent layer between stronger reflections across group 2 and into group 4 (Fig. 19). Reflection thickness variations above this layer indicate that wave-crest deposition rates decrease monotonically downslope. The thickness varies by a factor of 1.5 across the group 2 waves, and by nearly a factor of 2 from group 2 to group 4 (Figs. 19–21). We also measured the relative thickness of reflector sequences at the distal end of the wave field, taking advantage of continuous reflectors in group 4 (Fig. 22D). From the upslope side to the downslope side of Figure 22D the sequence thins by ~20%.

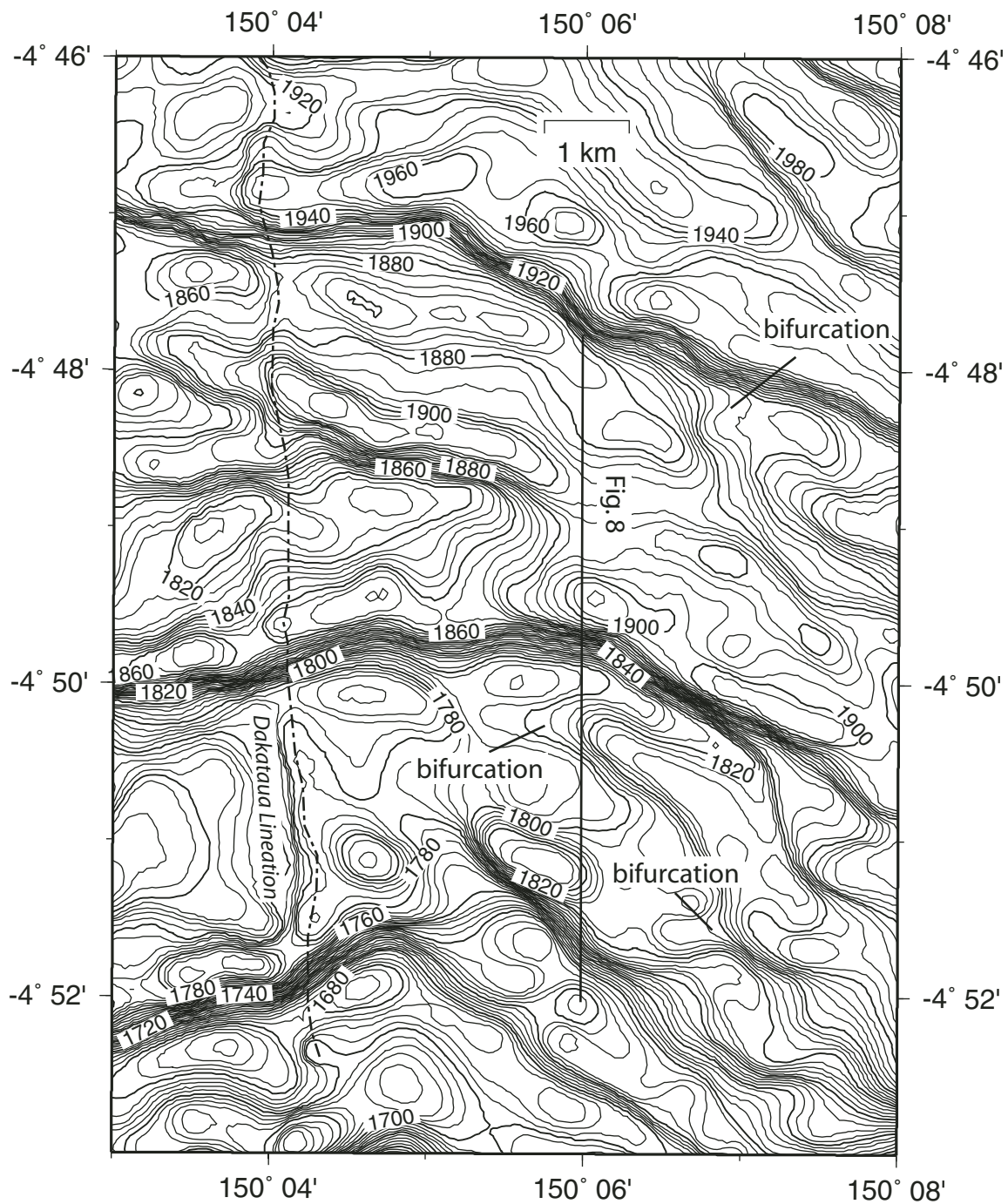


Figure 7. Bathymetry of Dakataua wave field, contoured at a 4 m interval, with annotated contours in bold every 20 m. Location of CHIRP line depicted in Figure 8 shown. The downslope sides are consistently steeper than the upslope sides of the features. Note the bifurcation near the center of the CHIRP line shown in Figure 8 and elsewhere. The Dakataua lineation is characterized by eastward-dipping slopes, widened depressions, and pinched-out wave crests.

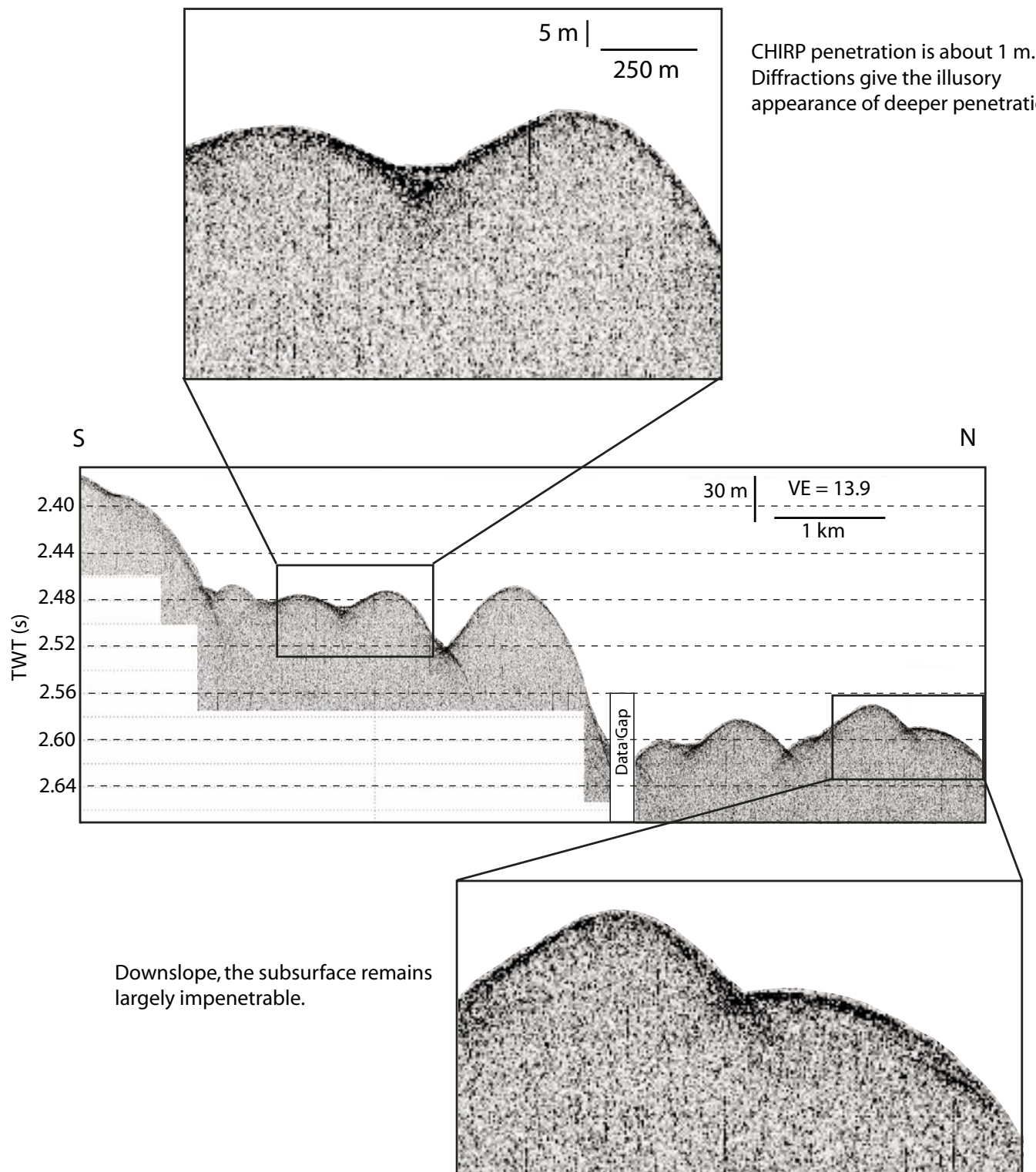


Figure 8. CHIRP profile of Dakataua wave field. Location shown in Figure 7. VE—vertical exaggeration; TWT—two-way traveltime. Detailed enlargements are at the same vertical exaggeration and 3.5 times the scale as the base figure. Both demonstrate the extremely limited penetration ( $\sim 1$  m) that characterizes this wave field.

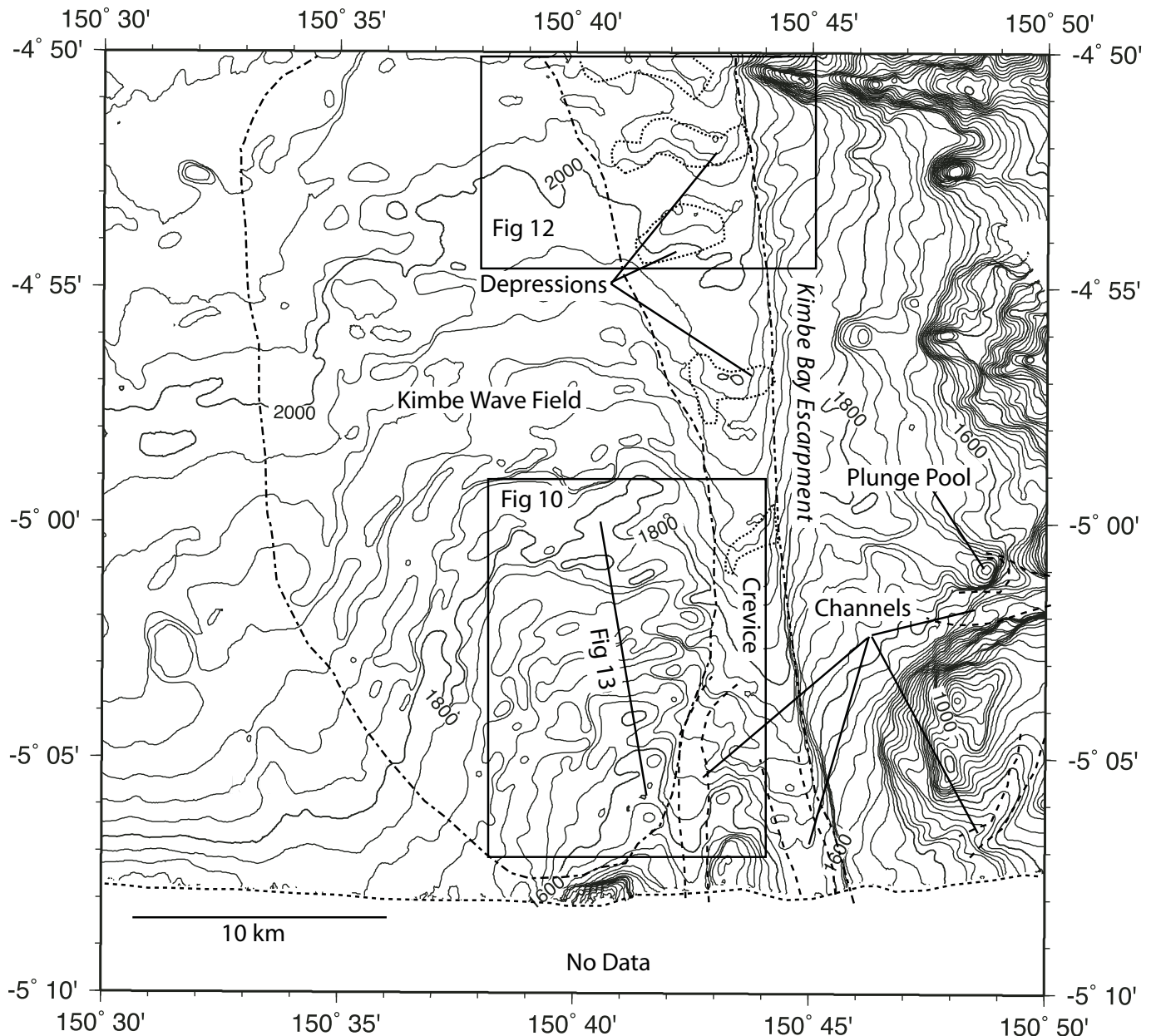


Figure 9. Bathymetry of the Kimbe Bay sediment-wave field. Contour interval is 25 m, with annotated contours in bold every 200 m. Side-scan mosaic of the same region at the same scale is shown in Figure 11. Motion along the newly discovered Kimbe Bay Escarpment is unknown. In the region between the escarpment and the wave field are several depressions associated with high backscatter. The outlines of these depressions correspond to regions of high backscatter. Detailed bathymetry and backscatter imagery of the pull-apart basins are shown in Figure 12. Locations of Figures 10 and 12 are shown. CHIRP line depicted in Figure 13 is shown.

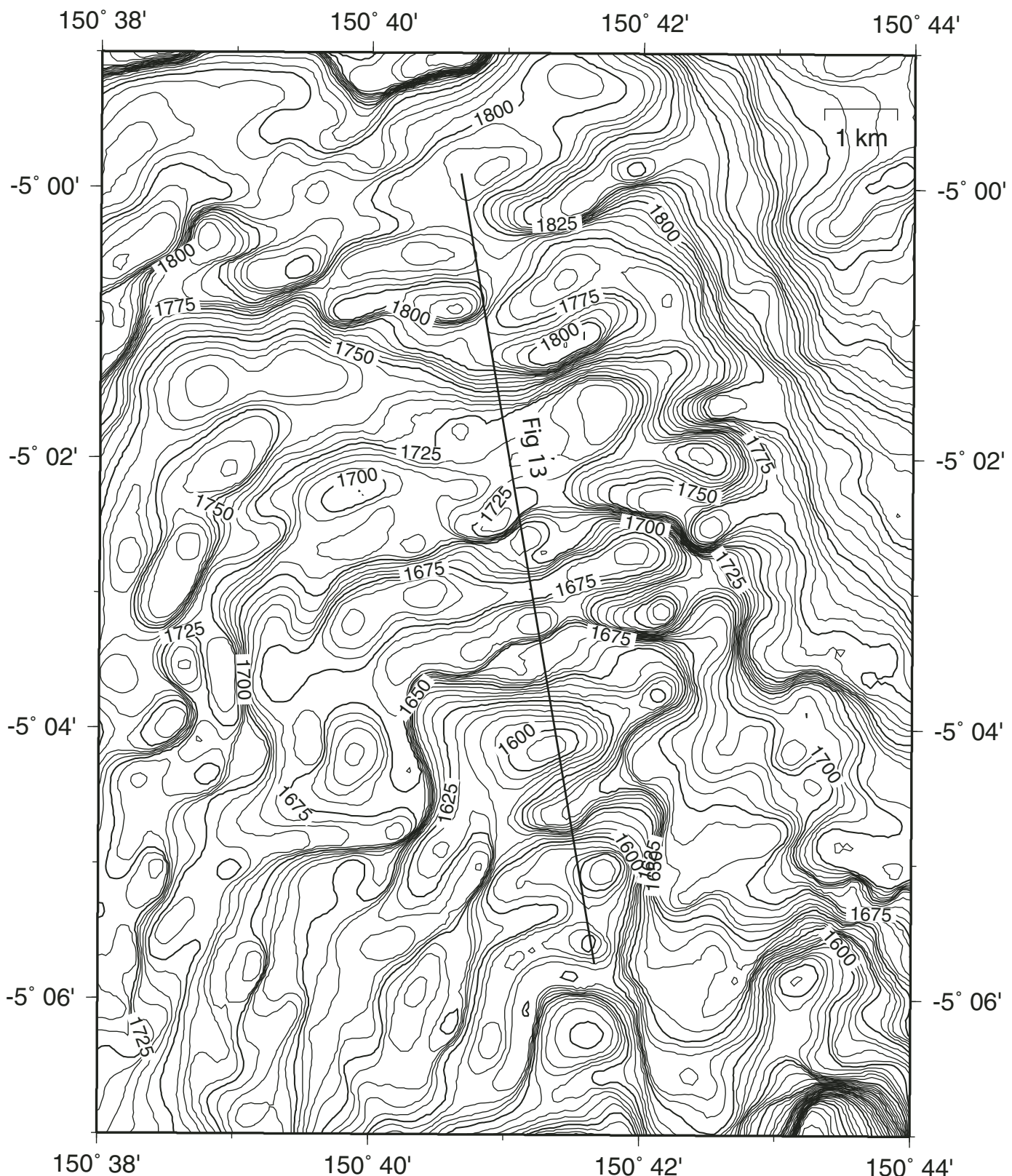


Figure 10. Detailed bathymetry of Kimbe Bay sediment-wave field. Contour interval is 5 m, with annotated contours in bold every 25 m. CHIRP line depicted in Figure 13 is shown; the scale of this line is 2.9 times that of Figures 9 and 11. Note the pronounced irregular morphology of the waves, with an overall arcuate pattern of alternating crests and troughs; superimposed on this is a chaotic assortment of peaks and valleys, resulting in highly sinuous structures.

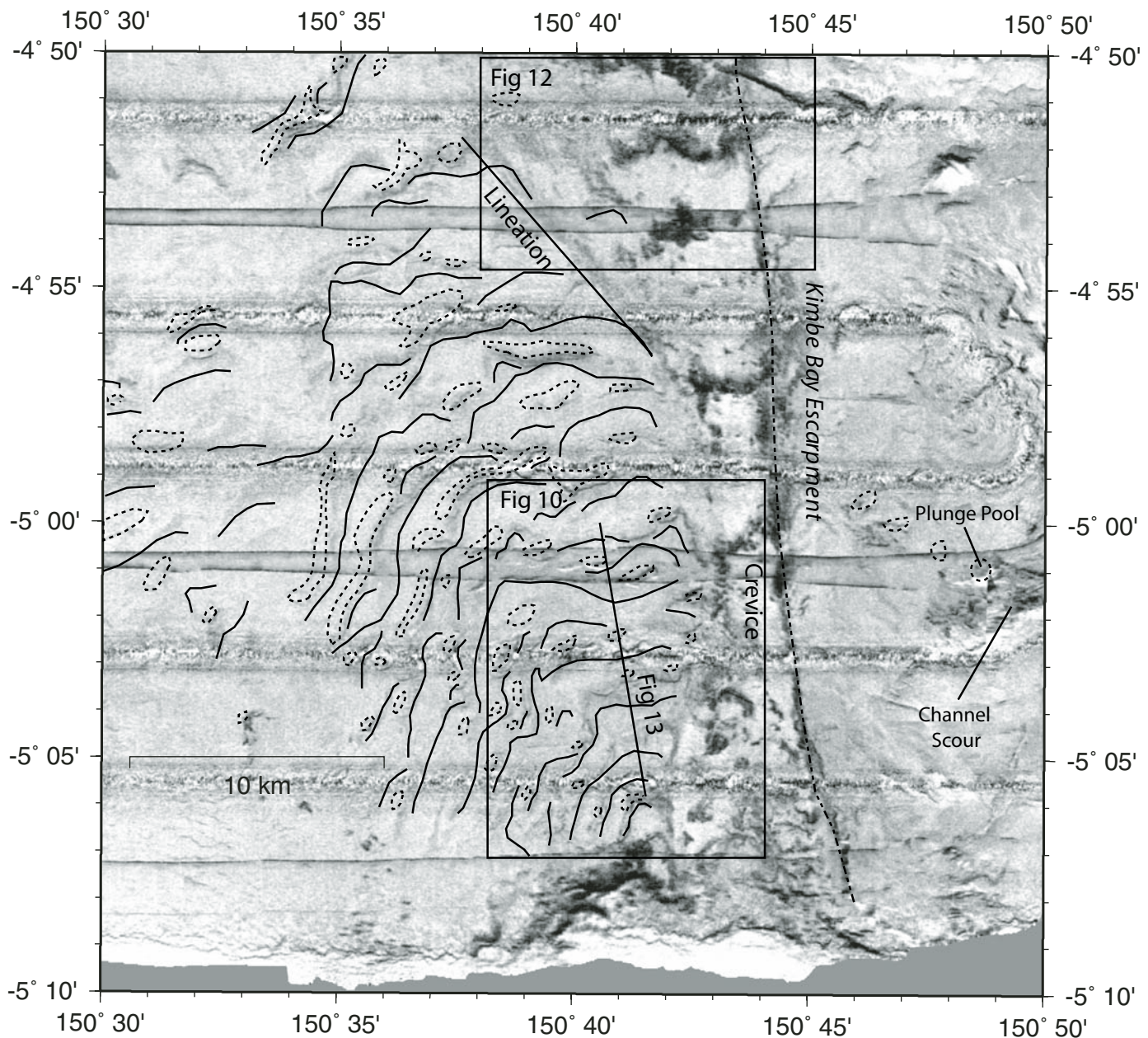


Figure 11. Side-scan mosaic of the same region depicted in Figure 9, and at the same scale. Dotted outline of field same as in Figure 9. Locations of Figures 10 and 12 are shown. CHIRP line depicted in Figure 13 is shown. Low backscatter is light, and high backscatter is dark. High-backscatter pattern within the wave field is associated with troughs. High-backscatter lineation is oriented  $33.7^\circ$  with respect to the general trend of the Kimbe Bay Escarpment. Solid lines denote the slope break between wave crests and steep downslope flanks of waves. Dashed lines denote enclosed depressions.

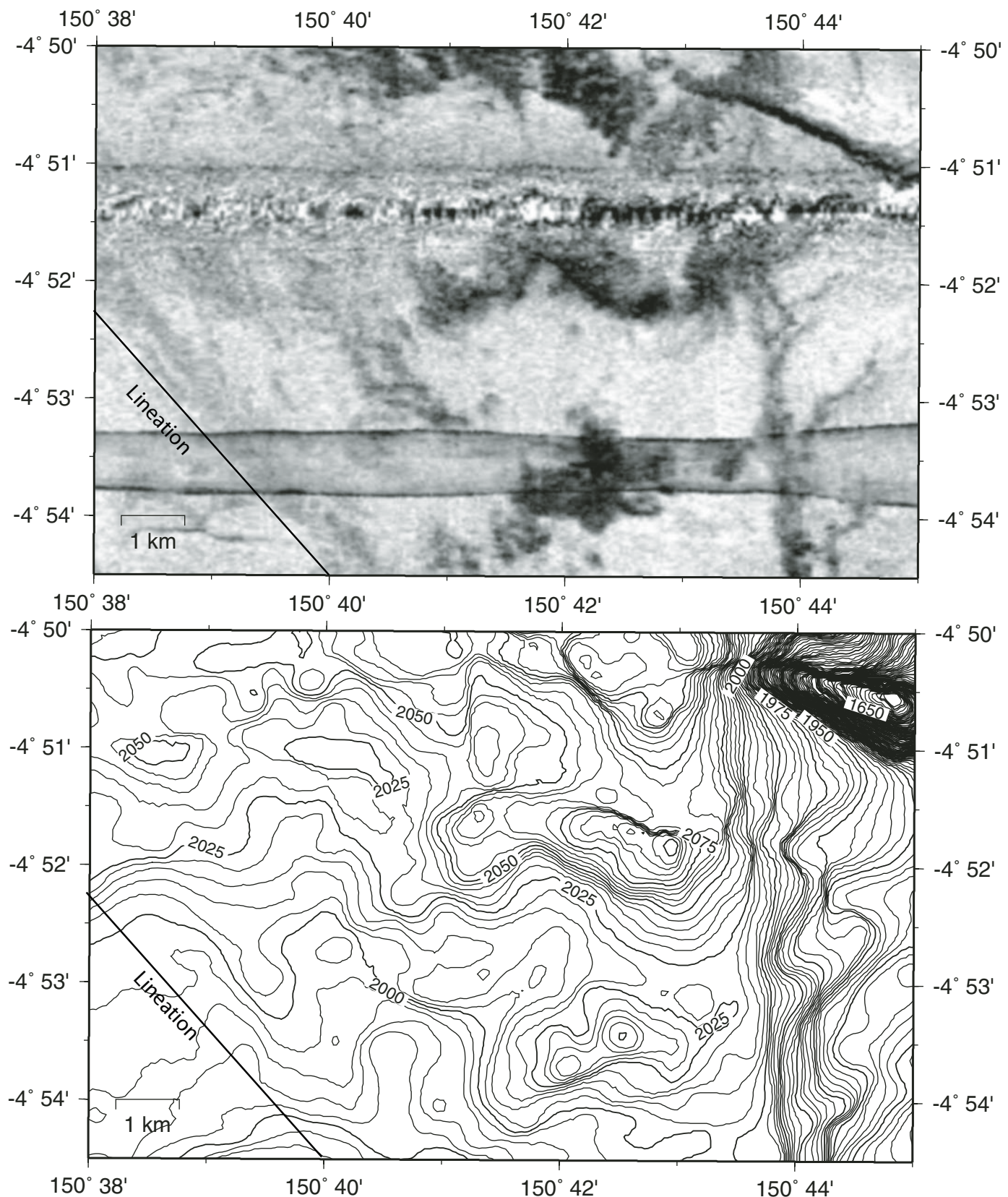
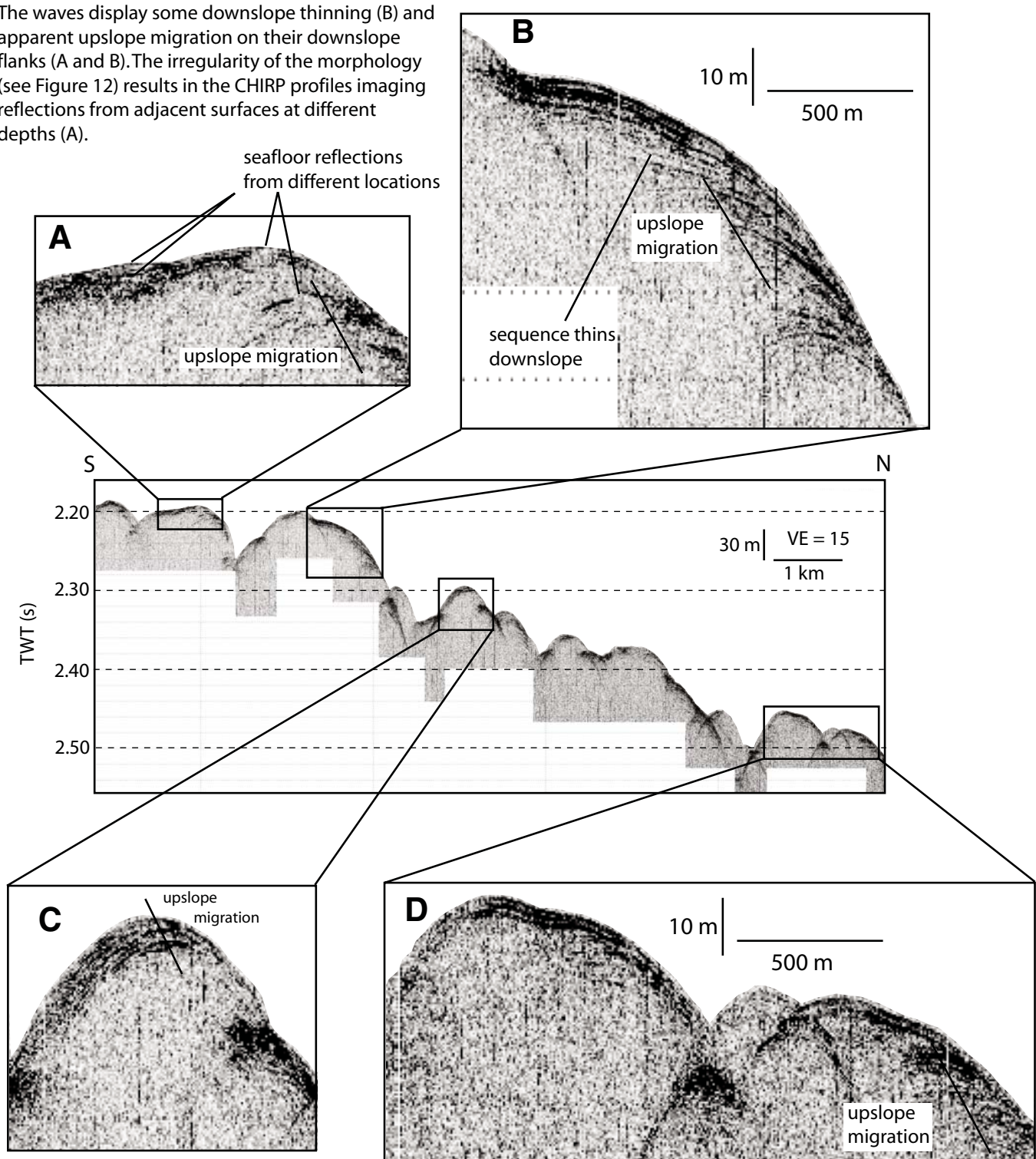


Figure 12. Close-up side-scan mosaic and bathymetry of enclosed depressions in the crevice, and the backscatter lineation noted in Figure 11. Contour interval is 5 m, with annotated contours in bold every 25 m. Scale is 2.8 times that of Figures 9 and 11.

The waves display some downslope thinning (B) and apparent upslope migration on their downslope flanks (A and B). The irregularity of the morphology (see Figure 12) results in the CHIRP profiles imaging reflections from adjacent surfaces at different depths (A).



Apparent upslope migration is present in most of the waves (C and D). In some cases this is true for the whole wave (C), but for most of the waves, upslope migration is only apparent on the steep, downslope flanks where it becomes difficult to distinguish between internal structure and diffractions (A, B, and D). Penetration varies widely from wave to wave, with some crests imaged to a depth of up to 6 to 8 m (B and C), and others only imaged to a depth of 2 to 3 m (A and D), suggesting sedimentation conditions are not consistent across the wave field.

Figure 13. CHIRP profile across a part of the Kimbe Bay wave field. Location shown in Figures 9, 10, and 11. VE—vertical exaggeration; TWT—two-way traveltimes. Detailed enlargements are at 4.2 times the scale and at the same vertical exaggeration as the base figure.

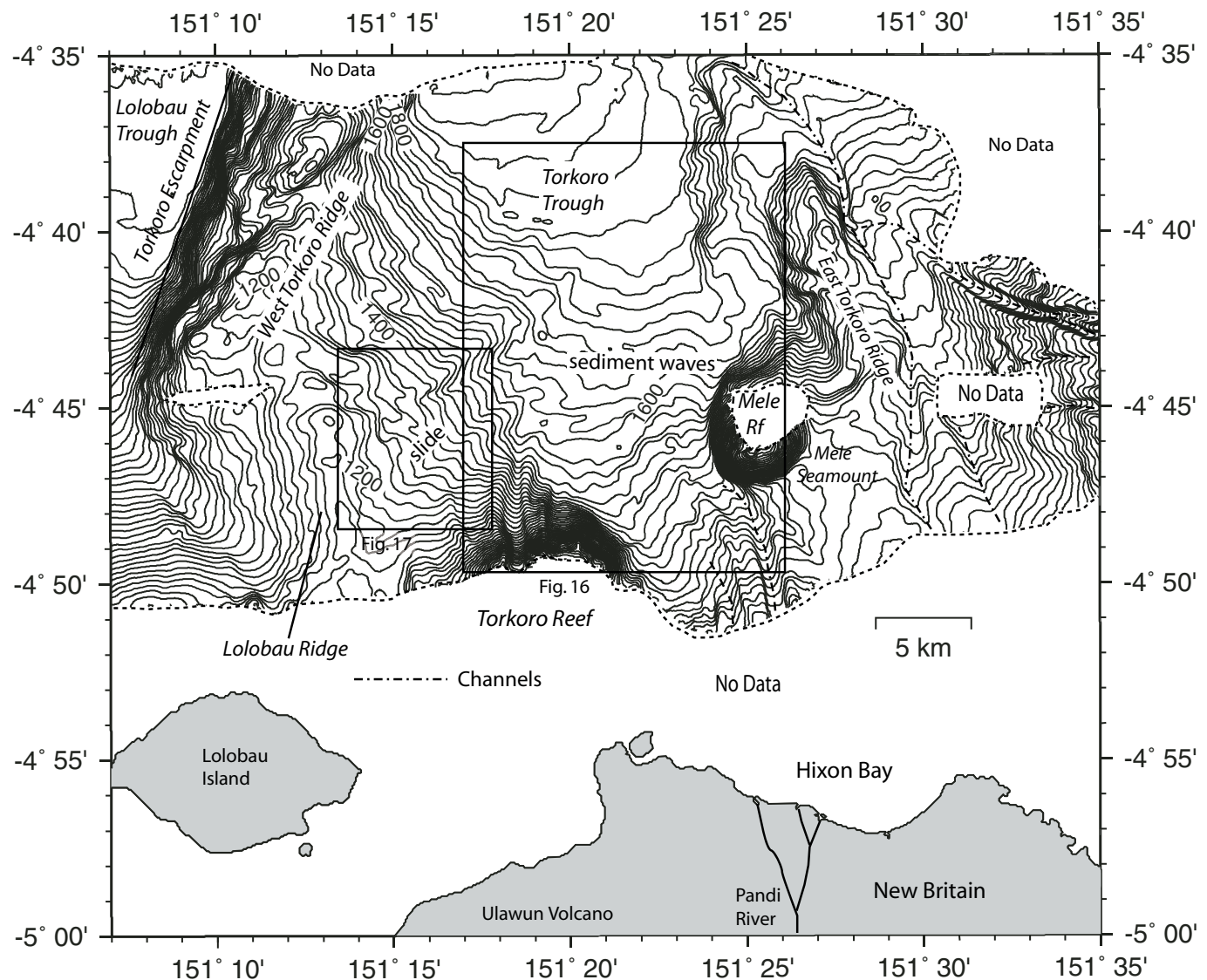


Figure 14. Bathymetry of the Hixon Bay region. Contour interval is 25 m, with annotated contours in bold every 200 m. Several channels feed into the imaged region, including those from the Pandi River, which drains part of the Nakanai Mountains (see Fig. 1) and Ulawun volcano. The Pandi River channels fade out as they enter the region between the Mele Seamount and Torkoro Reef. This is where a major sediment-wave field begins. This field is shown in more detail in Figure 16, the location of which is shown here. A slide scar is observed on the slope east of West Torkoro Ridge and Lolobau Ridge. This scar is shown in more detail in Figure 17, the location of which is shown here.

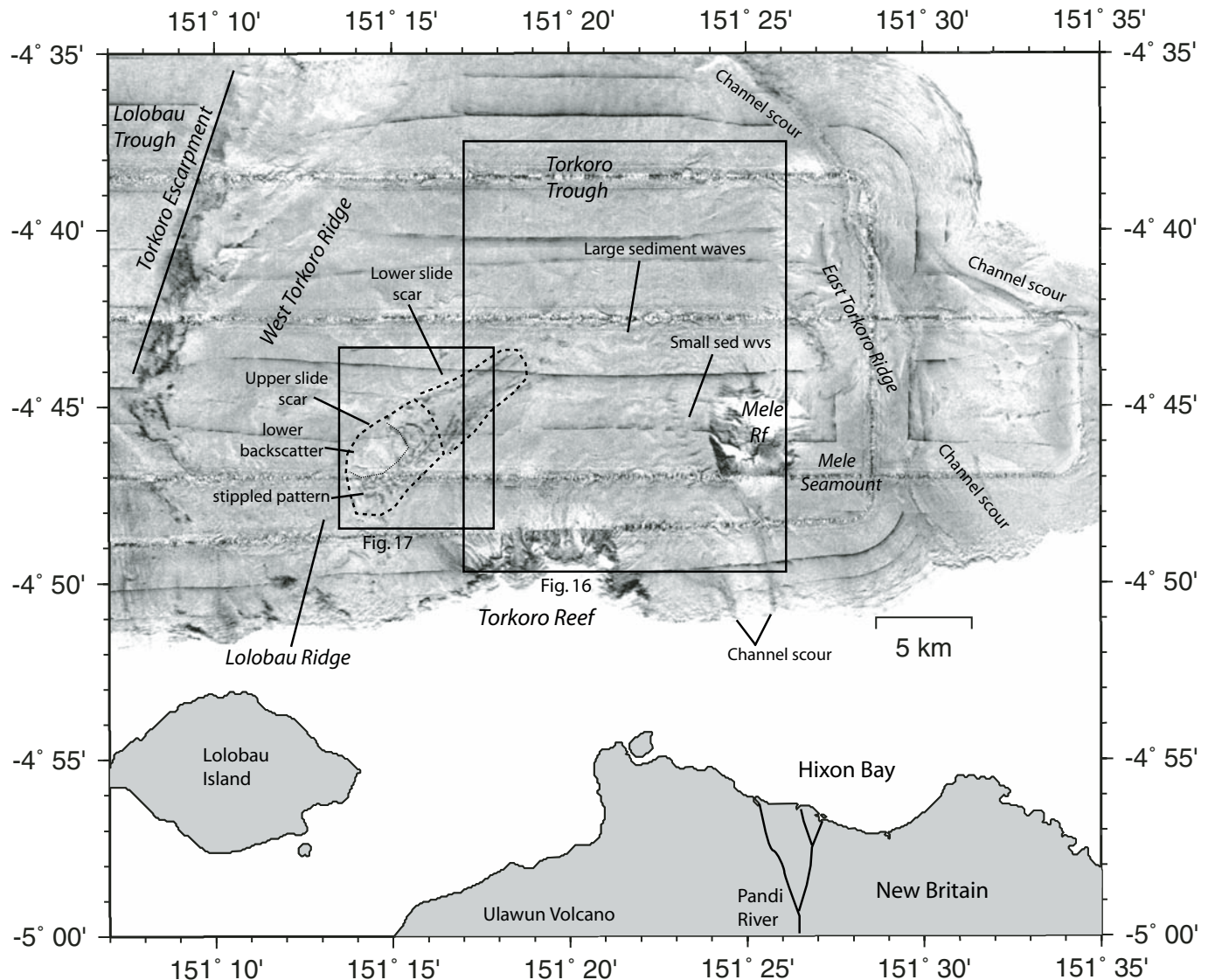


Figure 15. Hixon Bay area, with the location and scale the same as for Figure 14. Low backscatter is light, and high backscatter is dark. Regions without data are white. The slope of the Torkoro Escarpment is notably high in backscatter. The slide scar shows up clearly as a pattern of high backscatter. The backscatter pattern is distinctly different between the upper slide scar and the lower slide scar. The wave field within the box locating Figure 16 can be seen as a repetitive pattern of higher and lower backscatter. Both large sediment waves and small sediment waves can be seen. The large sediment waves are seen as a longer wavelength, lower contrast pattern, whereas the small sediment waves are seen as a shorter wavelength, higher contrast pattern. Channels are associated with high-backscatter scour.

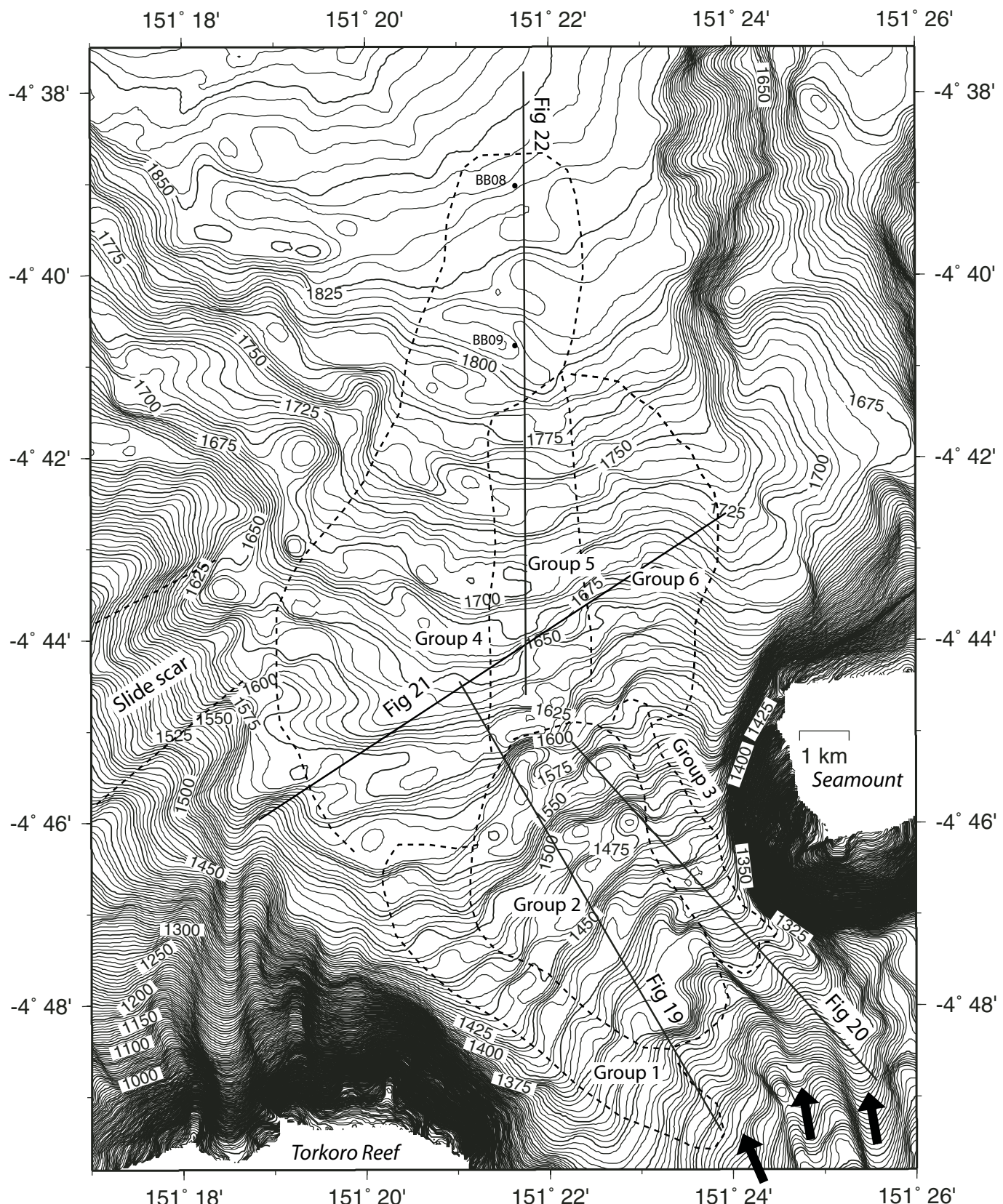


Figure 16. Bathymetry of the Hixon Bay main sediment-wave field. Contour interval is 5 m, with annotated contours in bold every 25 m. Sediment waves are divided into five groups, based on morphology. Locations of CHIRP profiles through sediment waves in Figures 19 through 22 are shown. Arrows highlight the channels that lead to the sediment-wave field. See text for details on the groups of waves. Core holes BB08 and BB09 are shown.

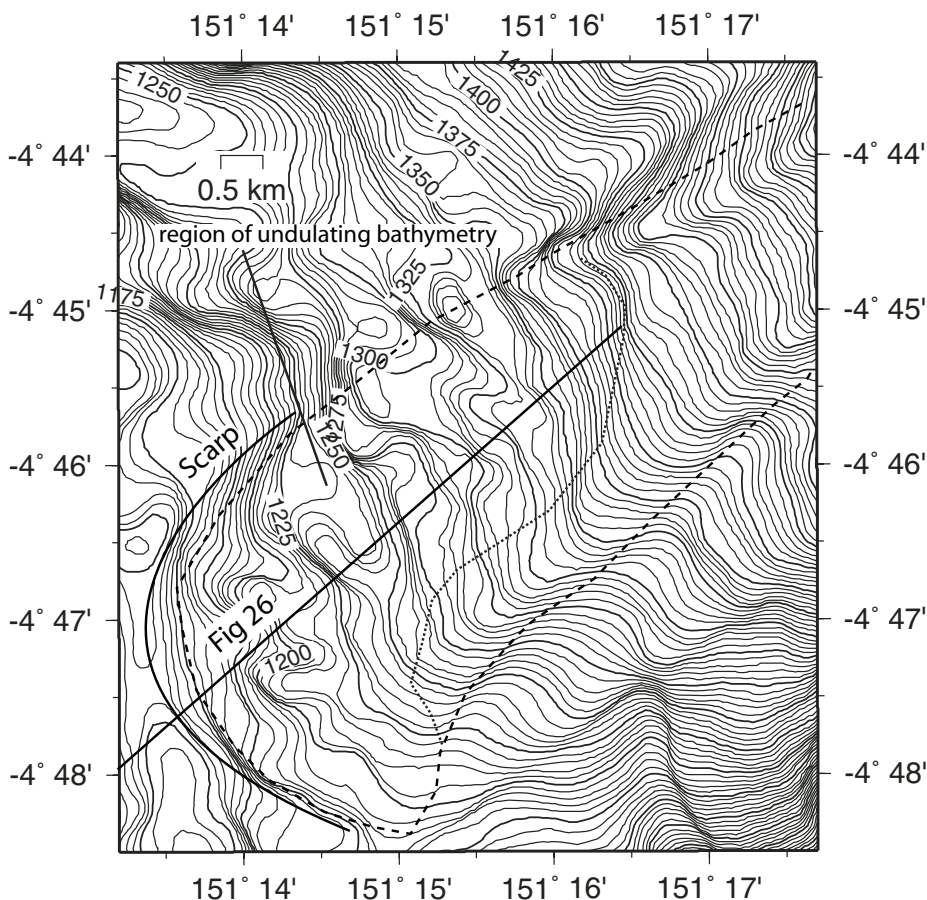


Figure 17. Detailed bathymetry of the slide scar in the Hixon Bay region. Contour interval is 5 m, with annotated contours in bold every 25 m. The slide scar and scarp are delineated with the dotted line. In the upslope portion of the scar, an undulating pattern is seen. A CHIRP line that cuts across these features is shown in Figure 25.

### Gravity Cores from the Hixon Bay Sediment-Wave Field

We collected two gravity cores to examine the nature of sediment being deposited and its rate of deposition. The core locations are shown in plan view in Figure 16 and in cross section in Figure 22. Core BB09 was taken in the trough between two waves, just upslope of a 1-km-wavelength, 20-m-high wave. The slope on which it is located dips <0.05° to the south. Core hole BB08 is 3.5 km downslope from core hole BB09 on the downslope flank of a wave near the very end of the field. The wave has a length of 1 km and a height of 10 m. The north-dipping flank of the wave on which core hole BB08 is located has a slope of 1°. Core BB09 is 164 cm long, and core BB08 is 85 cm long (Fig. 23). Depths in the cores are not corrected for compaction during collection.

Core BB09 penetrated through a unit of gray clay containing pumice dropstones (~130 cm; Fig. 23). Core BB08 penetrated into, but not through, this same unit (~80 cm). In both cores a series of silty and sandy tephras is interbedded with fine silt, silty clay, and clay units (Fig. 23). The well-sorted fine-black-sand tephra at 105 cm depth in core BB09 correlates physically with the well-sorted fine-black-sand tephra at 53 cm depth in core BB08 (Fig. 23). If this correlation holds, then the sedimentation rate between the clay-pumice unit and this tephra unit was slightly

lower in core BB09 than in core BB08. Subsequently, however, sedimentation would have been more rapid by nearly an order of magnitude in core BB09 than in core BB08, because of the correlation of the well-sorted fine white and black sand unit at 65 cm depth in core BB09 and at 42 cm depth in core BB08 (Fig. 23). In both cases, this white and black sand unit is topped with a pale gray clay unit that is slightly thicker in core BB08. Radiocarbon dating of planktonic foraminifers in core BB08 indicates that the white and black sand unit was deposited between 373 and 242 yr ago. The pale gray clay unit above it then took more than 200 yr to emplace, at a rate of roughly 0.5 mm yr<sup>-1</sup>.

Calibrated radiocarbon dates of planktonic foraminifers from both cores are shown plotted in Figure 24. The depths of the dates from each core have been normalized to the top of the well-sorted white and black sand layer we assume is from a single, discrete event affecting both sites. Ages in both Figure 23 and Figure 24 are given in years before 2004, when the cores were collected. Ages are taken from median probability dates, with upper and lower ranges shown.

Sedimentation patterns are broadly similar at the sites of cores BB08 and BB09, but in detail there are important differences, in particular the thickness of the pale clay layer above the white and black sand layer, the relative thicknesses between the

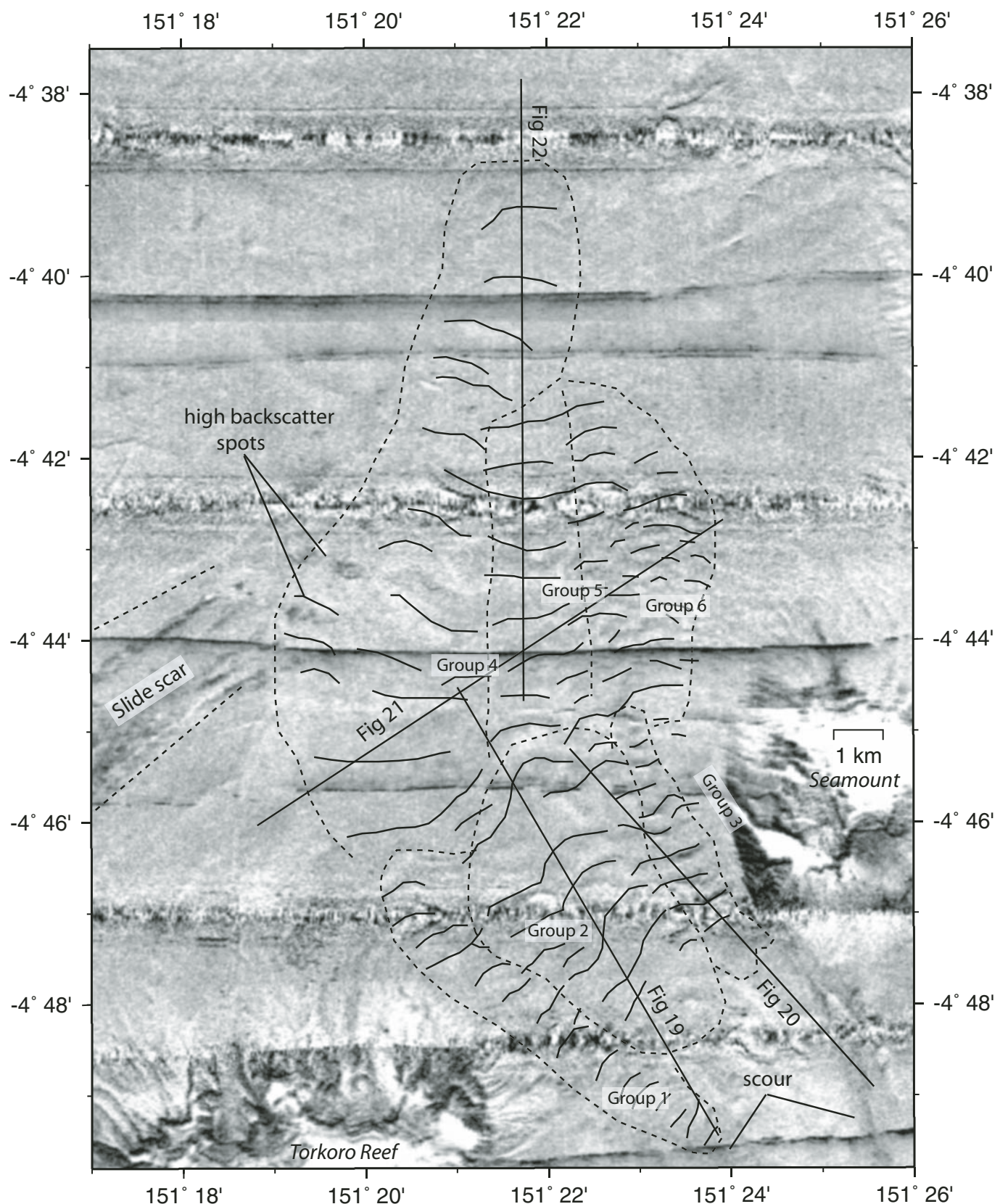


Figure 18. Side-scan mosaic of the central Hixon Bay region sediment-wave field. Dark tones are high backscatter. Region and scale are the same as for Figure 16. Locations of the CHIRP lines depicted in Figures 19 through 22 are shown. The different groups of waves in the sediment-wave field display different acoustic characteristics, with some groups displaying strong asymmetry between upslope and downslope flanks (groups 3 and 6), and others displaying weak or no asymmetry. High backscatter spots mark the slopes of a few group 4 waves nearest the slide scar.

TABLE 1. BACKSCATTER AND MORPHOLOGICAL CHARACTERISTICS OF HIXON BAY SEDIMENT WAVES

Group number	Wave length (m)	Wave height (m)	Backscatter contrast	Wave crests	Channel
1	600–800	20–30	None	Slightly sinuous	Yes
2	~1000	30–80	Faint	Somewhat sinuous	No
3	500, D.D.	20, D.D.	High	Linear or somewhat sinuous	Yes
4	1000–2000	30–40	High contrast spots near slide scar	Slightly sinuous	No
5	~1000	15–20	Faint	Slightly sinuous	No
6	100–500	10–20	Faint	Linear or slightly sinuous	No

Note: Backscatter contrast refers to the flanks of individual waves. Channel denotes whether the group is associated with a channel directly upslope. D.D.—decreasing downslope.

TABLE 2. SUB-BOTTOM PROFILE CHARACTERISTICS OF HIXON BAY SEDIMENT WAVES

Group number	Penetration depth (m)	Reflector character	Upslope migration	Continuous reflectors	Figure reference
1	<5	N.D.	N.D.	N.D.	19
2	Up to 20	Well stratified, D.T.	Yes	Between some waves	19, 20
3	<5	Primarily diffractions	N.D.	N.D.	20
4	Up to 20, less at distal end	Well stratified, D.T.	Yes	Between some waves, at distal end	19, 21, 22
5	~10	Well stratified, D.T.	Yes	Between some waves	21, 22
6	<5	Primarily diffractions	N.D.	N.D.	21

Note: D.T.—downslope thinning, meaning the sequence is observed to thin downslope; N.D.—no data, meaning the group was not imaged clearly in sub-bottom profiles.

well-sorted fine-black-tephra layer and the white and black sand layer, and the number of upward-fining units above the white and black sand layer (Fig. 23). The heterogeneity between the cores is not surprising because the wave field as a whole is heterogeneous, and sedimentation patterns vary across the field as a whole.

### Hixon Bay Region Slide

The upper part of the Hixon Bay slide contains undulating features, and sediment dispersed from slope failures within the slide scar may deposit on the distal end of the sediment-wave field (Fig. 17). The slide scar is apparent but diverges from a half-circle shape in its southern end. A clearly defined chute runs downslope toward Torkoro Trough, although part of the northern boundary of this chute is obscured by undulations that compose most of the upper part of the slide scar. These undulations are reminiscent of the sediment waves discussed above, with a wavelength of roughly 1 km and wave heights of up to 40 m. Either side of the slide chute appears as a channel ~5 m deeper than the center of the chute (Fig. 17).

In side-scan imagery these channels are associated with high backscatter streaks (Fig. 15). The waveforms appear as alternating high and low backscatter regions, with the steeper, downslope flanks associated with high backscatter. Where the overall slope is flattest the contrast in backscatter is much less.

In profile, one wave shows clear upslope migration (Fig. 25). The complex morphology and slopes of up to 4° within the slide scar prevent clear imaging of the field with a shallow-towed CHIRP system. The downslope end of the slide scar also appears to have been buried (Fig. 16).

### DISCUSSION

Based solely on the criteria given in O’Leary and Laine (1996), H.J. Lee et al. (2002), and Wynn and Stow (2002), all of the imaged wave fields fail simple classification. Nonetheless, they provide important clues to the origins of sediment-wave fields. Sediment waves, although well-recognized features, are not ubiquitous but form only under very specific conditions. Once the origin of a given wave field has been established, it yields important information on broader processes.

### Tolokiwa Sediment-Wave Fields

The upslope migration and acoustic asymmetry observed in the large sediment waves northeast of Tolokiwa suggest a current origin. The dimensions of the waves and the average slope of the field are consistent with either a turbidity-current origin or a bottom-current origin. The region is seismically active, and so the low slopes (<0.5°) are also consistent with a deformational origin, but the fields are not immediately associated with a fault.

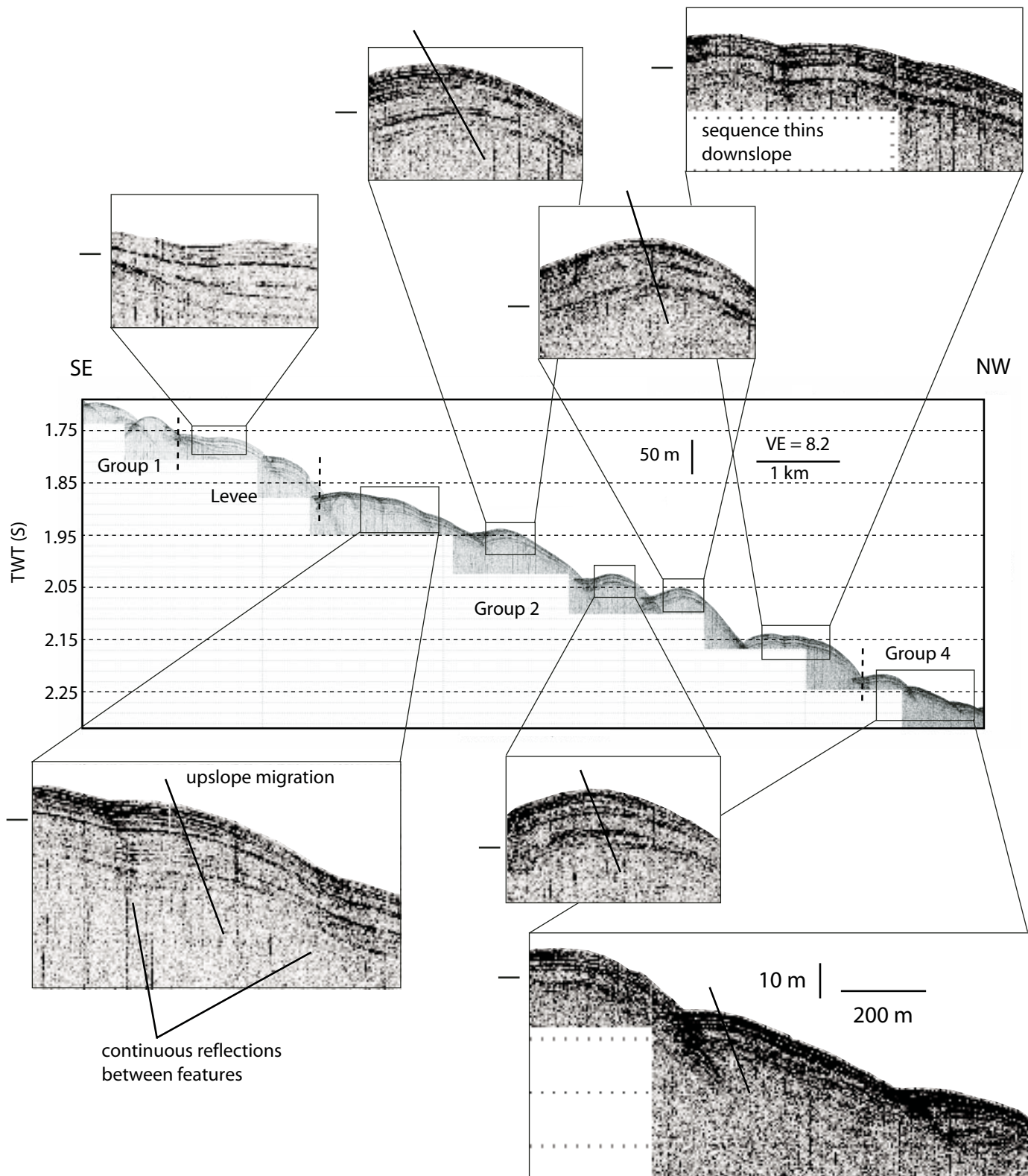


Figure 19. CHIRP line across Hixon Bay sediment waves. Location shown in Figure 18. Detailed enlargements are at the same vertical exaggeration and at 5.1 times the scale of the central base figure. The black tick marks indicate a transparent layer between a series of reflections that is correlated throughout this part of the wave field. Angled lines highlight upslope migration in the wave field. This CHIRP line transects a small part of group 1, a small levee, group 2, and a small part of group 4. VE—vertical exaggeration; TWT—two-way traveltimes. The thickness of deposits above the transparent layer increases upslope from ~5 m in group 4 to 6 m at the bottom of group 2 to 9 m at the top of group 2. This measurement is for the thickness at the wave crest and assumes a sound velocity of  $1500 \text{ m s}^{-1}$ .

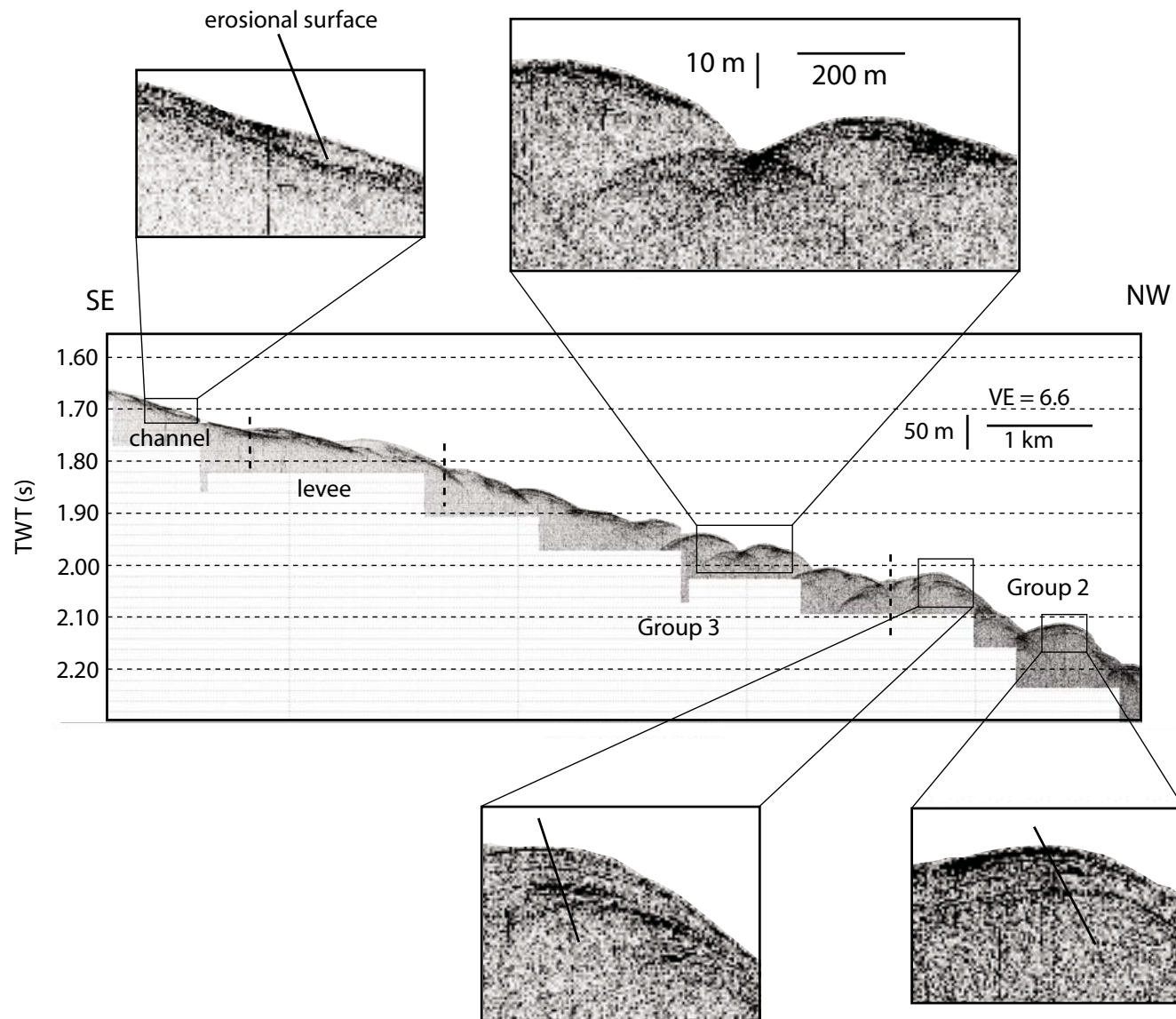


Figure 20. CHIRP line across the Hixon Bay sediment-wave field. Location shown in Figure 18. The line begins within the channel leading to group 3. It then crosses the levee of the channel at a highly oblique angle. The line then crosses the largest waves of group 3. Because the group 3 waves are small, diffractions dominate the CHIRP image. Penetration in the group 3 waves is also <5 m. The group 2 waves display upslope migration, as highlighted by the angled lines. VE—vertical exaggeration; TWT—two-way traveltme.

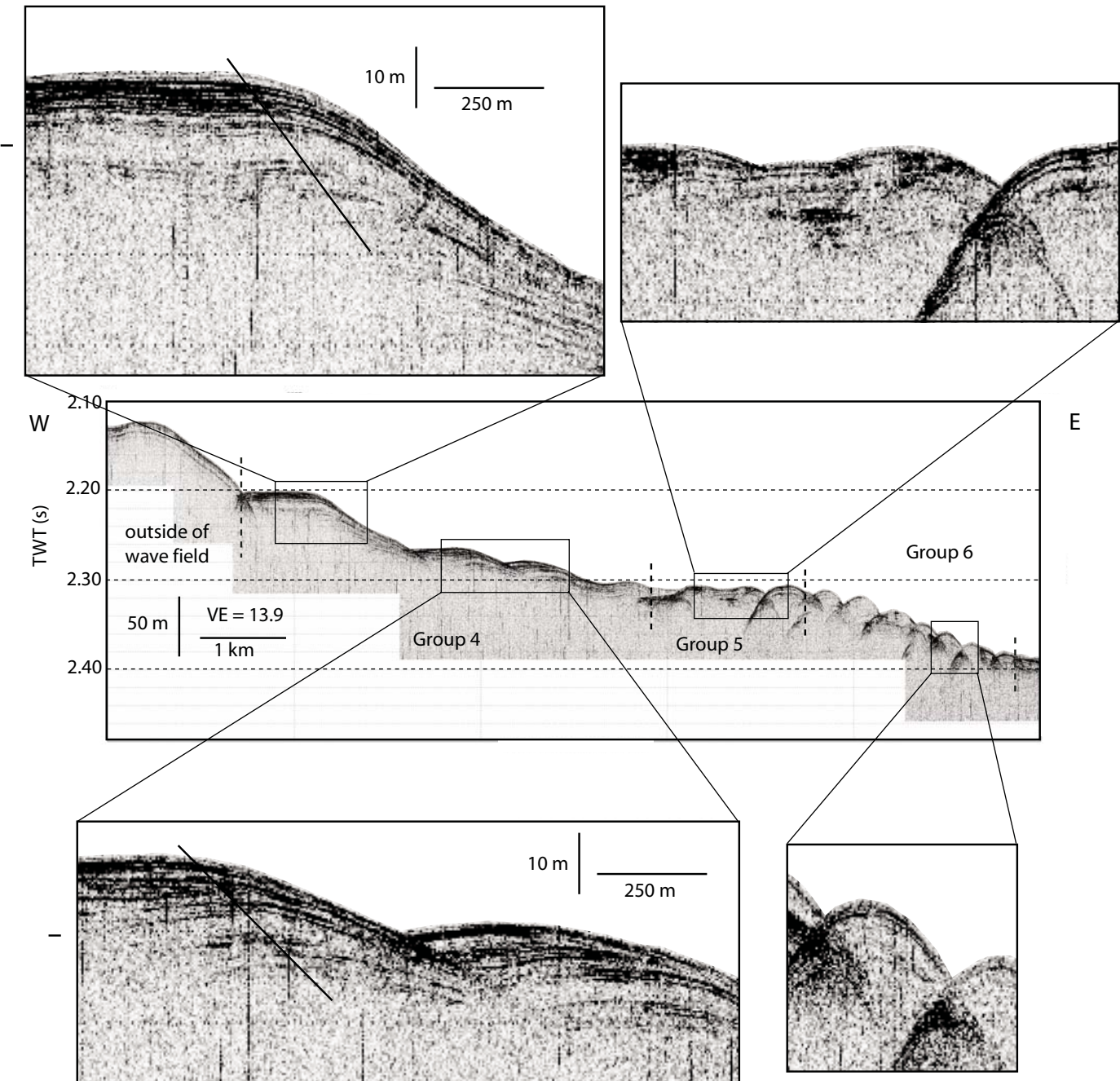


Figure 21. CHIRP line across the Hixon Bay sediment waves. Location shown in Figure 18. This line cuts obliquely across the southern end of group 4, group 5, and the central part of group 6, and slightly beyond. The tick marks indicate a transparent layer that we interpret to be the same transparent layer seen in Figure 19. VE—vertical exaggeration; TWT—two-way traveltimes. The group 4 waves appear to display upslope migration, as highlighted by the angled lines. Note the decreasing penetration from group 4 to group 5 to group 6.

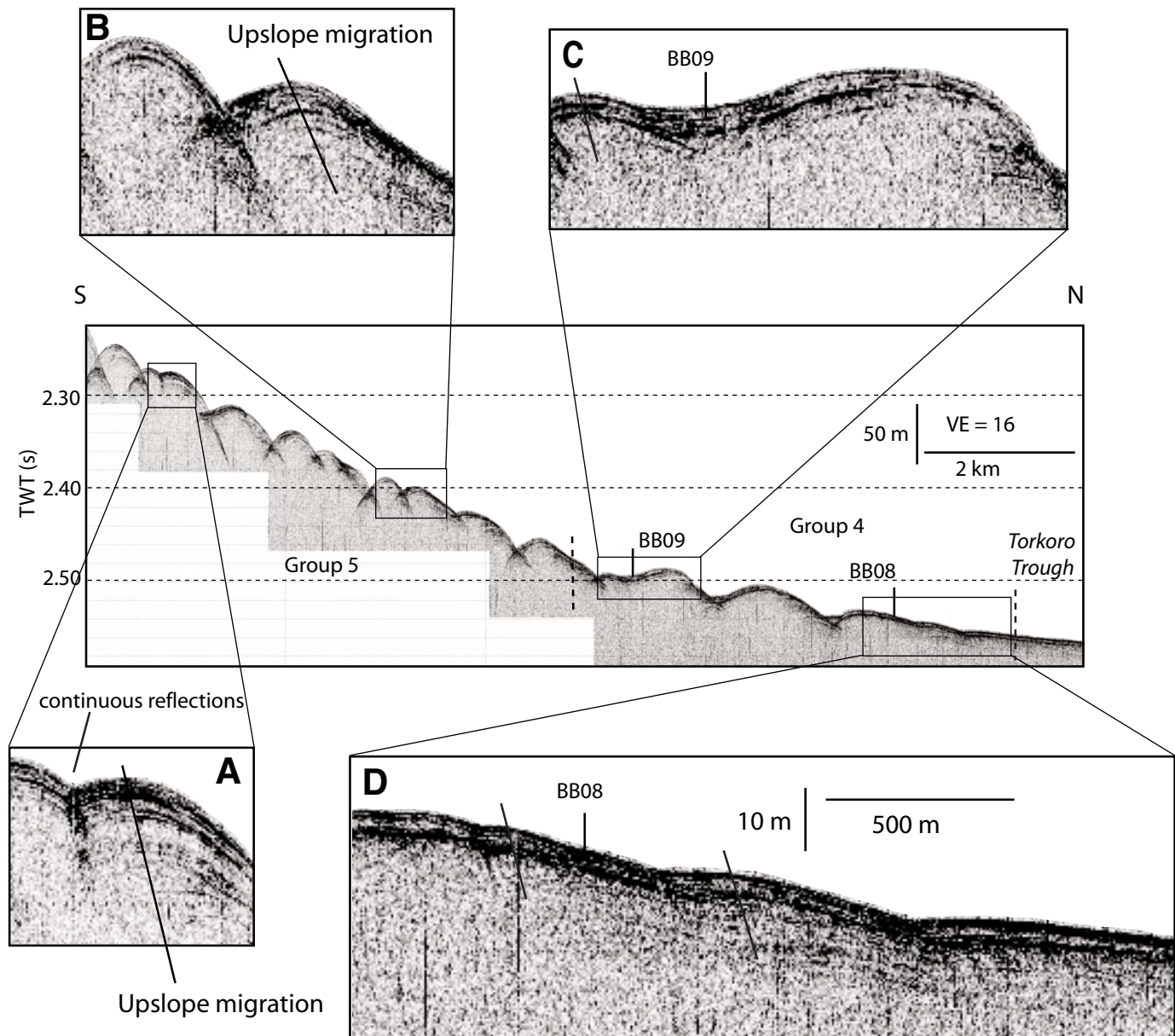


Figure 22. CHIRP profile of Hixon Bay sediment wave field. Location shown in Figure 18. VE—vertical exaggeration; TWT—two-way travel-time. Core holes BB08 and BB09 are shown. This line crosses the group 5 waves perpendicular to their crests. Each of these waves displays clear upslope migration, as shown in the two enlargements (A and B). In the group 4 waves shown here, upslope migration can be seen (angled line in panels C and D). Also apparent is a downslope thinning of the sequence. Reflections in panel D are continuous and grade into parallel reflections in Torkoro Trough, and thin by ~20% from the upslope-most wave in panel D to the downslope-most wave. This thinning is also seen when comparing cores BB08 and BB09 (see Fig. 23).

Depth (cm)

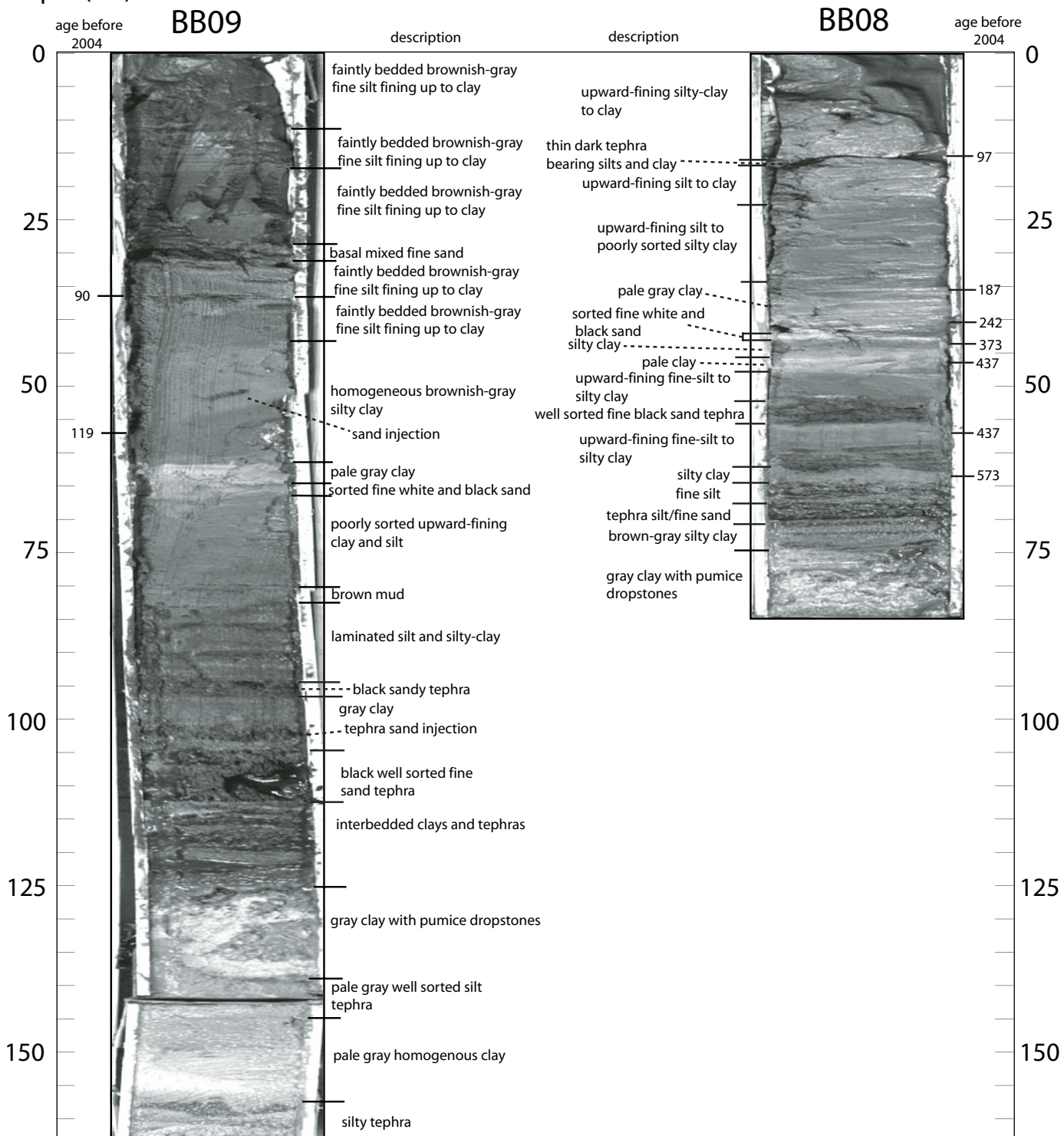


Figure 23. Cores BB09 and BB08 from the Hixon Bay region sediment-wave field, with calibrated radiocarbon ages of planktonic foraminifers. Both cores penetrated a gray clay unit containing pumice dropstones. Above this unit is a series of tephra deposits and silt, silty clay, and clay deposits. Both units contain a thin layer of well-sorted white sand with black grains (65 cm depth in core BB09, and 42 cm depth in core BB08), topped by a unit of pale gray clay. Ages (in years before 2004) from this pale gray clay unit indicate that it was deposited slowly in comparison with the upward-fining silt and clay units found above it in both cores. Depths are uncorrected for compaction of sediment during core collection.

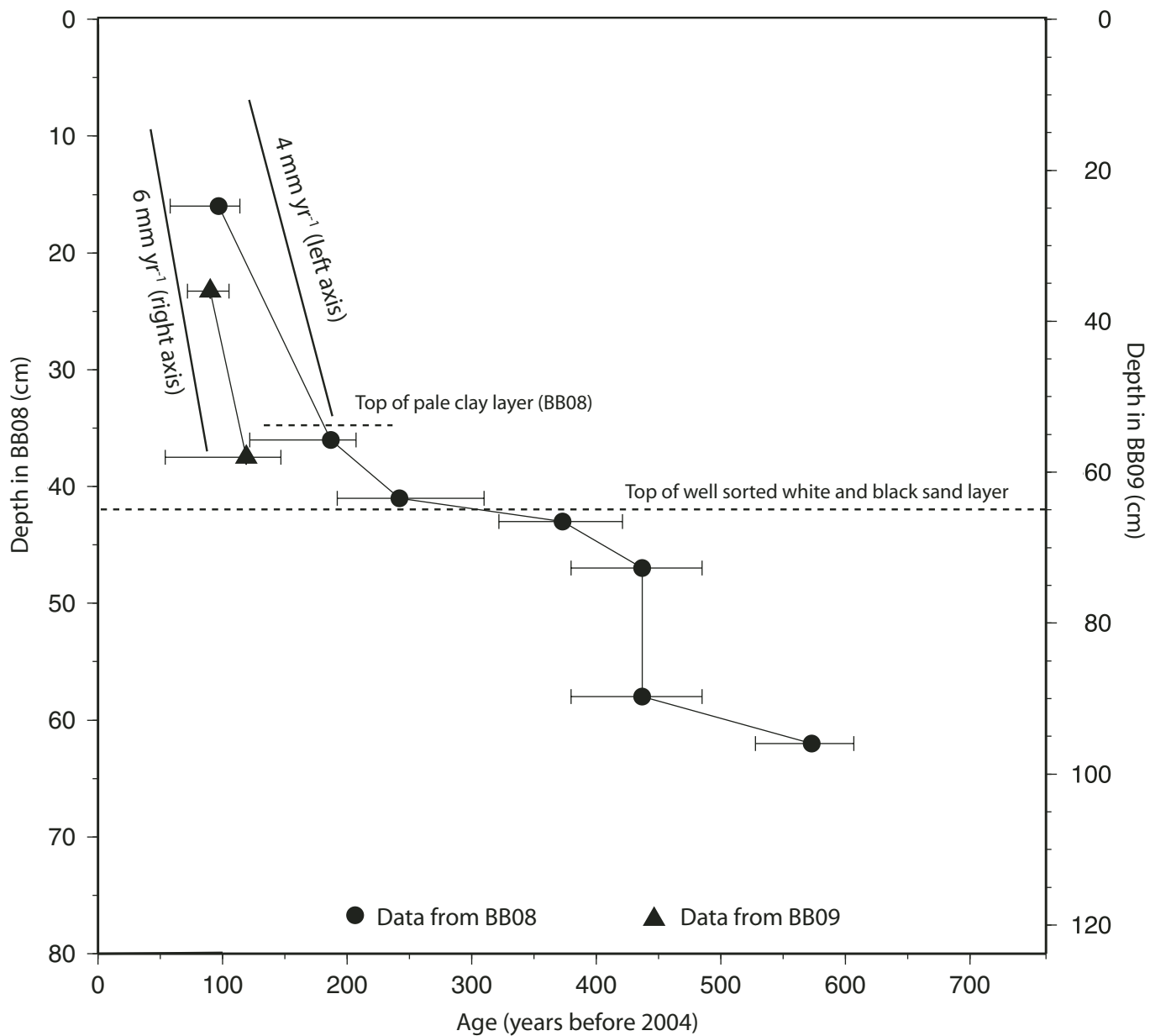


Figure 24. Depth-age plot of radiocarbon dates from planktonic foraminifers from cores BB08 and BB09 in the Hixon Bay sediment-wave field. Age is in years before 2004, when the cores were collected. Depths have been normalized to the top of the well-sorted white and black sand layer we observe in both cores, and which we assume is from a single, discrete event affecting both sites. Depth within core BB08 is shown on left axis. Depth within core BB09 is shown on right axis. Median ages are shown, with upper and lower ranges shown. For comparison, lines corresponding to example sedimentation rates for each axis are drawn. The sedimentation rate for core BB09 since the late nineteenth century is  $\sim 6 \text{ mm yr}^{-1}$ . The average sedimentation rate for core BB08 since the event that produced the white and black sand layer is about two-thirds the average sedimentation rate in core BB09 since the same event. Thus,  $4 \text{ mm yr}^{-1}$ , using the scale of the left axis, is shown.

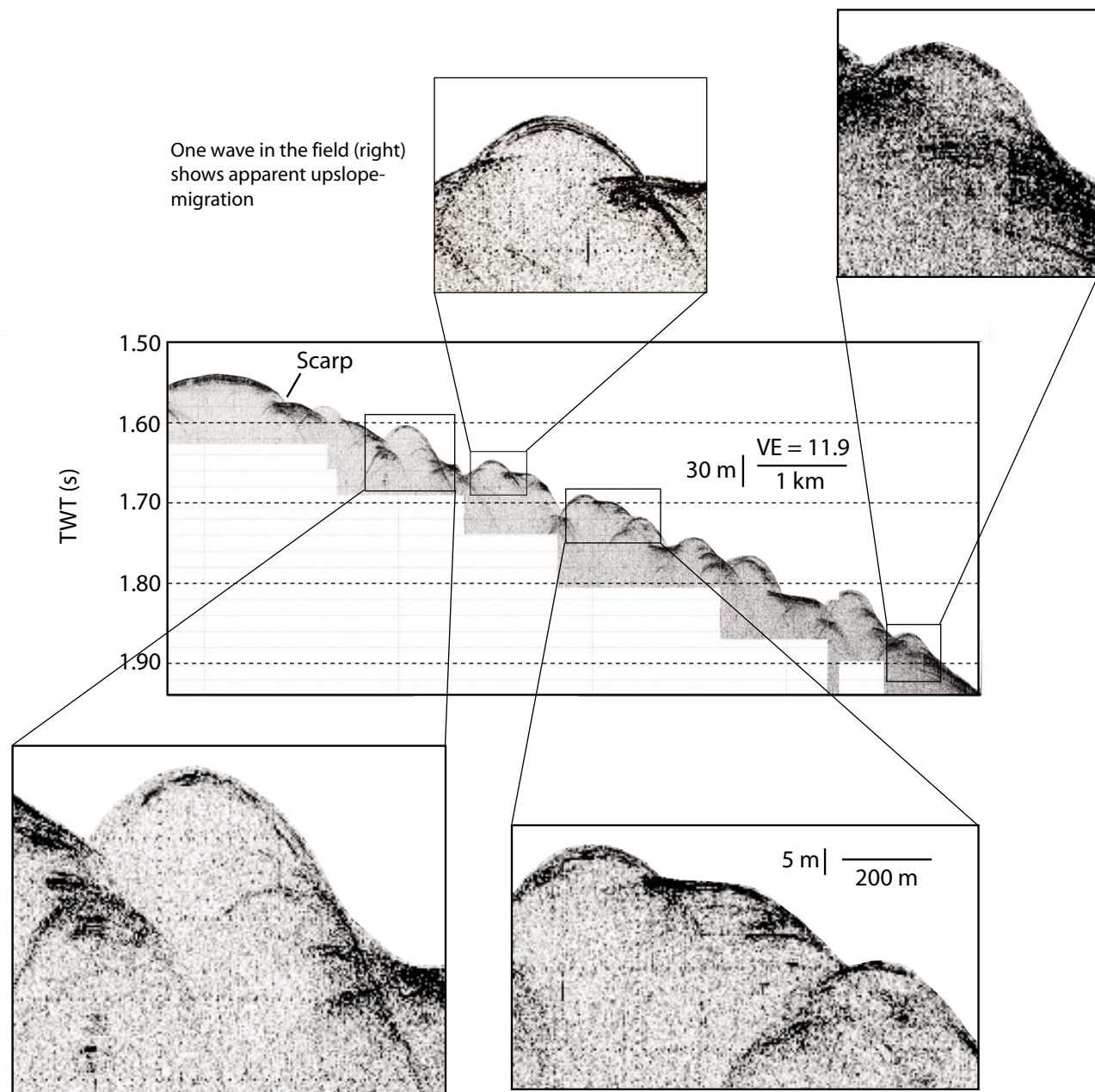


Figure 25. CHIRP line through Hixon Bay slide. Detailed enlargements are at the same vertical exaggeration and at 5 times the scale of the base figure. VE—vertical exaggeration; TWT—two-way traveltimes. Upslope migration is clear only in one wave in this field. Location of figure shown in Figure 17.

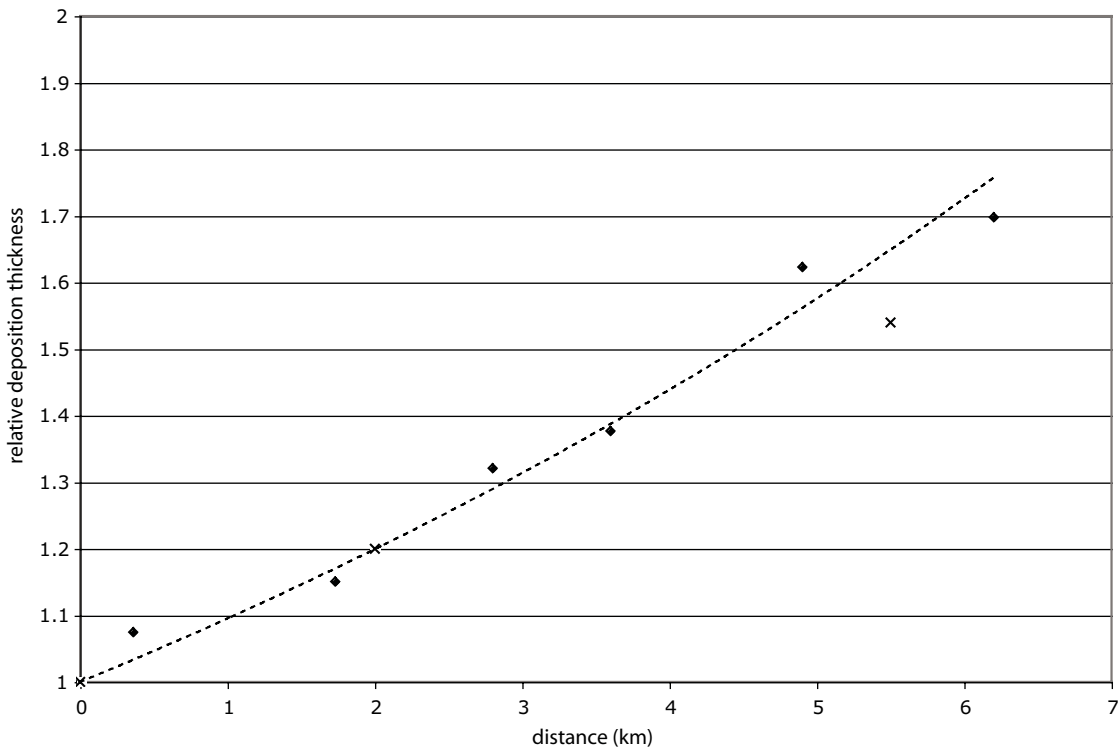


Figure 26. Plot of relative deposition thickness on wave crests in the Hixon Bay sediment wave field as a function of relative distance. Measurements are taken from seven wave crests shown in Figure 19, normalized to the thickness of the most distal wave crest measured. These are plotted as diamonds. Three measurements are taken from wave crests in the distal end of the waves shown in Figure 22, plotted as crosses. These measurements are also normalized to the most distal wave crest in the set. Distance is kilometers upslope from the most distal measurement in the set. The proximal measurement from Figure 22 (the cross at 5.5 km) is extrapolated to the wave crest from the site of core hole BB09 and assumes a relative sedimentation rate at the site of this core hole of 1.55 times the sedimentation rate at the site of core hole BB08. The plot shows that these two sets of measurements, which are separated by 10 km, are consistent with a downslope exponential decay of sedimentation rate from wave crest to wave crest. Short-dashed line shows an exponential curve with a characteristic decay length of 7.6 km.

We interpret that some of the small waves are younger features than the large waves, owing to the onlapping contact that the small waves have with the large waves. Nevertheless, other small waves interspersed with the larger waves could have formed concomitantly. Because of their acoustic asymmetry, and the oblique orientation of their wave crests with respect to local gradients, we interpret the small waves to be of bottom-current origin. The lack of evidence for turbidity-current activity in the vicinity of the wave fields is consistent with this interpretation.

The origin of the large waves remains inconclusive. We suggest, however, that the consistent upslope migration more likely indicates a current origin than a deformational origin. The nearest possible source of turbidity currents to the field is debris flows from Tolokiwa, but the orientation of the waves is inconsistent with currents flowing from south to north. One alternative is that the large waves were also generated by bottom currents. In this case, the differences in morphology between the large waves and small waves would imply a difference in bottom-current

velocity and direction, and possibly a change in density stratification within the ambient seawater (Flood, 1988). However, the crests of the large waves are oriented perpendicular to the local slope, suggesting that they were formed by turbidity currents derived from shallow regions to the west. The small waves thus may have formed subsequent to or concomitantly with the large waves as they were modified by bottom currents.

#### Dakataua Sediment-Wave Field

Features in the Dakataua wave field suggest both a deformational origin and a turbidity-current origin. The decreasing wave height with distance from the caldera (Fig. 5), combined with the decreasing high backscatter scour features in side-scan imagery (Fig. 6), suggest that turbidity currents may play a role. The field is isolated from hyperpycnal currents, however. The wave field begins ~5 km from shore, south of a steep slope that drops more than 1200 m in this space. We suggest that coastal erosion by

energetic waves during large storms could result directly in turbidity currents as sediment is concentrated in the surf zone during peaks of storm activity and then released during lulls in wave action (Scully et al., 2002). Energetic waves could also result in turbidity currents by destabilizing the slope of the caldera, resulting in numerous small slope failures of weakly consolidated sediment that rapidly entrains seawater to become a turbidity flow (Marr et al., 2001). Additionally, ashfall from eruptions can result in a hyperconcentrated sediment layer on the sea surface, which can result in turbidity currents (Fiske et al., 1998; Parsons et al., 2001). Lastly, turbidity flows could be triggered by earthquakes. Turbidity-current-generated sediment waves proximal to volcanic sources but lacking fluvial input are recognized elsewhere (Wynn et al., 2000).

The arcuate and irregular morphology of the waves, as well as the large enclosed depressions in the field, suggest that deformation of some kind may play a role in the formation of these sediment waves. The Dakataua lineation (Fig. 7) may be a fault with some degree of downthrow to the east. We suggest that the Dakataua wave field is formed by some combination of turbidity currents and deformation. Lacking sub-bottom data, however, the origin of the features remains speculative.

### **Kimbe Bay Sediment-Wave Field**

The Kimbe Bay wave field is far from a potential source of hyperpycnal currents. The highly irregular and relatively arcuate plan-view morphology and the many enclosed depressions in the field suggest a deformational origin. The waves display some subsurface characteristics of current activity, however (Fig. 13), in upslope migration of the wave crests. The presence of nearby channels and plunge pools indicates that turbidity currents are active in the vicinity of this field. The crevice to the east of the field may be related to motion along the Kimbe Bay Escarpment if this is an active fault, or the crevice may be the site of focused channel flow. The depressions in the crevice may be tectonically controlled, although without subsurface imagery we cannot confirm this interpretation. The lineation in the field (Fig. 11) may be the site of a splay fault related to the Kimbe Bay Escarpment.

Like the Dakataua field, the Kimbe Bay field forms a topographic high relative to the surrounding seafloor, suggesting higher sedimentation rates within the field. The two fields are also similar in terms of wave height, wavelength, the presence of deep enclosed depressions within the fields, and irregular morphology. Both fields are closely related to signs of turbidity-current activity and possible faults. We suggest that the Kimbe Bay field is also formed by a combination of turbidity currents and deformation, although we cannot determine which process dominates.

### **Hixon Bay Sediment-Wave Field**

The morphological heterogeneity of this sediment-wave field suggests that different parts of the field formed under different conditions. However, the groups we have defined are not

entirely distinct from one another, with some wave crests continuous through the boundaries of two or more groups (Fig. 18). This overlap suggests that either the morphology predates deposition by currents or that currents interact with topography, depending on their magnitude, and that a continuum of magnitudes and slightly different flow paths will result in indistinct boundaries between flow conditions, giving rise to the variability in the morphology of the field. Hyperpycnal currents that originate from the Pandi River will tend to follow the channels leading toward the wave field, as seen by the high backscatter scour in these channels (Fig. 18).

A turbidity-current origin for the Hixon Bay sediment waves is strongly supported by sub-bottom data. The similarity of reflections from wave to wave (Figs. 19–22), the progressive downslope thinning of reflection sequences (Figs. 19, 22), the continuity of reflections between waves (Figs. 19, 22), and the ubiquitous upslope migration of waves (Figs. 19–22) all argue against a deformational origin and in favor of a current origin. Torkoro Trough is enclosed on three sides (Fig. 14). Cores taken from the sediment-wave field show a series of upward-fining, graded units consistent with turbidites (Fig. 23). These observations argue against a bottom-current origin and in favor of a turbidity-current origin of the wave field. The heterogeneous flow conditions across the wave field may be largely the result of focused flow down the channels and different magnitudes of flow events.

The high-backscatter regions within the slide scar (Fig. 25) and the high-backscatter spots on the upslope flanks of three sediment waves near the base of the slide scar (Fig. 18) suggest active sediment transport through the slide scar. Some of this sediment may reach the distal portion of the sediment-wave field. However, the undulating topography in the upslope part of the slide scar (Fig. 17) implies a site of active deposition. This deposition, together with the large, mountainous drainage area of the Pandi River in comparison with the catchments of rivers draining the east flank of Lolobau or the west flank of Ulawun, and also the absence of channels or turbidity scour leading toward the slide scar, all suggest that hyperpycnal discharge from the Pandi River is the dominant source for the upward-fining units in the cores. Slope failure and turbidity flows caused by rapid sedimentation and triggered by earthquakes also may explain some of the heterogeneity of the field. We conclude that the Hixon Bay sediment-wave field is of hyperpycnal-current origin, at least insofar as active growth is concerned. We cannot determine whether or not the field grew from initial topography created by some other process.

### **Sediment Supply to the Hixon Bay Sediment-Wave Field**

The Hixon Bay sediment-wave field demonstrates that significant quantities of sediment are capable of reaching the Kimbe Bay wave field, >40 km from shore. The Hixon Bay sediment-wave field covers ~70 km<sup>2</sup> (Fig. 16). The waves display a pattern of decreasing deposition downslope. Using a transparent layer

that can be correlated through much of the field, we measured the relative thicknesses of deposits on seven wave crests (Fig. 19). Farther downslope in the distal end of the field, we measured three more by tracing continuous reflections (Fig. 22D) and by extrapolating the difference in sedimentation rates observed in cores BB08 and BB09 to the wave crest nearest core hole BB09 (Fig. 22C), taking advantage of continuous reflections between this core and the wave crest.

Although flow conditions vary throughout the field, we assume that sediment is primarily, although not exclusively, originating as discharge from the Pandi River. The similarity of cores BB08 and BB09 (Fig. 23) and the similarity of reflection sequences from wave to wave in groups 2, 4, and 5 (Figs. 19–22) are consistent with this assumption. We assume no discontinuities in sedimentation rate between groups. That reflector thickness decreases steadily downslope from wave to wave, even between groups (Figs. 19, 22) is consistent with this assumption. The waves display upslope migration, with thicker upslope sediment deposits and thinner downslope sediment deposits. We assume that the thickness of sediment at a wave crest is approximately the average sediment thickness for a given wave. We normalize the seven measurements of thickness from Figure 19 to the thickness measurement of the wave crest farthest downslope in this set. We similarly normalize the three measurements of thickness from the distal end of the wave field (Fig. 22). Lastly, we assume a power-law distribution of hyperpycnal-current events from the Pandi River (Warrick and Milliman, 2003; Dadson, et al., 2005). Thus, deposition rates are greater in the upslope part of the wave field because this region receives sediment from many small, frequent events as well as from large, infrequent events, whereas the downslope part of the wave field receives sediment only from the large, infrequent events (H.J. Lee et al., 2002).

A power-law distribution of events is expected to produce an exponential decay of sedimentation rates away from the source. We find that the two sets of normalized relative-thickness measurements are consistent with a single exponential decay rate (Fig. 26). Linear functions will also fit both sets of measurements. However, linear functions are not invariant to scalar multiplication. Because we are normalizing each set of measurements, a single linear function cannot fit both sets. The characteristic decay rate of an exponential function, however, is invariant to scalar multiplication. The characteristic decay length of this curve is ~7.6 km. That is, from wave crest to wave crest, sedimentation rates are inferred to decrease by half 7.6 km downslope from any given point in the field. Based on the above assumptions, we extrapolate this decay rate to the remainder of the field and calibrate it with sedimentation rates inferred from radiocarbon dating of cores BB08 and BB09 (Fig. 24).

Because we are interested in modern discharge of the Pandi River, we use only the upper parts of the cores, estimating sediment accumulation in the distal end of the field at  $4 \text{ mm yr}^{-1}$  (Fig. 24). Note that this estimate does not account for compression of the cores during collection and so is a lower bound estimate. However, some of this is likely to be pelagic sedimentation, and

some of this may be related to currents flowing down the Hixon slide scar (Fig. 25). Thus, we conservatively halve this estimate of sediment flux arriving from the Pandi River. Integrating, the average deposition rate for the whole field is  $\sim 5 \text{ mm yr}^{-1}$ . Multiplying by the area of the field, this yields a volumetric deposition of  $3.5 \times 10^5 \text{ m}^3 \text{ yr}^{-1}$ . Assuming a bulk density of the sediment of  $2200 \text{ kg m}^{-3}$  results in a mass deposition rate of  $7.7 \times 10^5 \text{ t yr}^{-1}$ . If this estimate represents a significant portion of Pandi River discharge, then it places a testable lower bound on the sediment supply of this system.

We cannot characterize the uncertainty in this estimation, but it suggests that a large part of the Pandi River sediment bypasses the Papua New Guinea shelf and is deposited in deep water. Because we observe sedimentation rates of  $>4 \text{ mm yr}^{-1}$  nearly 40 km from shore, we conclude that fluvial sediment entering Kimbe Bay can easily account for the deposition we observe in the Kimbe Bay wave field, although probably not the morphology itself. The rivers entering Kimbe Bay are smaller than the Pandi River, on the whole, and 40 km from shore the Hixon Bay sediment-wave field is dying out, not just beginning, as is the case in Kimbe Bay. Thus, although the Kimbe Bay field may be dominantly of turbidity-current origin, it is probably not of hyperpycnal-current origin.

We note that previous work has suggested that as much as 90% of sediment from the Sepik River may bypass the shelf as sediment gravity flows (Walsh and Nittrouer, 2003). This inference was based on a comparison of sediment discharge from the Sepik and measurements of depositional thickness on the shelf. The measured thickness of deposits only accounted for 10% of expected discharge. A similar argument was made by Dadson et al. (2005) regarding sediment discharged at hyperpycnal concentrations from the Choshui River in Taiwan. The Hixon Bay sediment waves present the opposite side of the story for the Pandi River. Results from this field suggest that on active tectonic margins with narrow shelves, hyperpycnal flows play an important role in delivering sediment to the ocean. This may be capable of explaining missing shelf deposits elsewhere, such as off the Sepik River, the Choshui River, and the Eel River (Walsh and Nittrouer, 2003; Dadson, et al., 2005; Sommerfield and Nittrouer, 1999).

## CONCLUSIONS

We image six sediment-wave fields in the Bismarck Volcanic Arc. The two Tolokiwa fields appear to have formed by turbidity currents and were subsequently or concomitantly modified by bottom currents. The Kimbe Bay and Dakataua wave fields appear to be of deformational and turbidity-current origin. In Hixon Bay, two hyperpycnal-current-generated sediment-wave fields are observed. One is a small, apparently young field in its initial stages of growth. The other field is an older, more stable feature related to discharge from the Pandi River. Measurements from this wave field indicate that a large part of sediment discharge from the Pandi River is deposited in deep water.

The evidence for turbidity currents in the vicinity of the Dakataua and Kimbe Bay wave fields, and that both fields are topographic highs relative to the surrounding seafloor, suggest focused deposition within the area of these wave fields. Between these fields and the Hixon Bay wave fields, sediment waves with turbidity-current components of formation appear to be a common feature in the Bismarck Volcanic Arc, particularly where sedimentation rates are relatively high. In these locations, deposition rates can vary greatly in the space of a few kilometers, both along the strike of the arc because of focused sedimentation, and across the strike because of the variation of sedimentation rates between the upslope and downslope flanks of a sediment wave. Thus, care must be taken when applying interpretations of a sedimentary section to the remainder of the arc environment.

Between these fields and the Tolokiwa fields, we do not observe large sediment waves. Topographic relief in this region is lower than in eastern New Britain, and so we expect that sedimentation rates are significantly lower. Thus, sediment waves with turbidity-current contributions to formation may be an indicator of relatively high sedimentation rates, although the inverse may not be true. We are not aware of large turbidity-current sediment waves that are recognized in the sedimentary record. This is probably due largely to an inherent difficulty in recognizing such large, subtle features from outcrops, particularly if the sequence is at all deformed. Sections in which high sedimentation rates have been recognized thus may be good places for reexamining the sedimentary record for sediment-wave fields.

## ACKNOWLEDGMENTS

Funding for this research was provided by the Marine Geology and Geophysics section of the U.S. National Science Foundation, grant OCE-0327004 to E. Silver and S. Ward, and grant OCE-0328278 to N. Driscoll. We are grateful for the advice and support of many people in carrying out this research, including Hugh Davies, James Robins, Bruce Appelgate and the Hawaii Mapping Research Group, Russell Perembo and Susan John of the University of Papua New Guinea for picking foraminifers, Michael Kashgarian of the radiocarbon facility at Lawrence Livermore National Laboratory for assistance with dating, the Oregon State University coring team, and the captain and crew of the research vessel *Kilo Moana*. We thank A. Draut (Associate Editor), H. Lee, J. Sample, and K. Straub for their thorough and insightful reviews of this manuscript. Most of the figures for this paper were generated in part using Generic Mapping Tools.

## REFERENCES CITED

- Abbott, L.D., Silver, E.A., Thompson, P.R., Filewicz, M.V., Schneider, C., and Abdoerrias, 1994, Stratigraphic constraints on the development and timing of arc-continent collision in northern Papua New Guinea: *Journal of Sedimentary Research*, v. 64, p. 169–183.
- Bowen, A.J., Normark, W.R., and Piper, D.J.W., 1984, Modeling of turbidity currents on Navy submarine fan, California Continental Borderland: *Sedimentology*, v. 31, p. 169–185, doi: 10.1111/j.1365-3091.1984.tb01957.x.
- Coleman, S.E., Zhang, M.H., and Clunie, T.M., 2005, Sediment-wave development in subcritical water flow: *Journal of Hydraulic Engineering*, v. 131, p. 106–111, doi: 10.1061/(ASCE)0733-9429(2005)131:2(106).
- Dadson, S., Hovius, N., Pegg, S., Dade, W.B., Horng, M.J., and Chen, H., 2005, Hyperpycnal river flows from an active mountain belt: *Journal of Geophysical Research*, v. 110, p. F04016, doi: 10.1029/2004JF000244.
- Ercilla, G., Belén, A., Wynn, R.B., and Baraza, J., 2002, Turbidity current sediment waves on irregular slopes: Observations from the Orinoco sediment-wave field: *Marine Geology*, v. 192, p. 171–187, doi: 10.1016/S0025-3227(02)00554-6.
- Faugères, J.-C., Gonther, E., Mulder, T., Kenyon, N., Cirac, P., Gribouillard, R., Berné, S., and Lesuavé, R., 2002, Multi-process generated sediment waves on the Landes Plateau (Bay of Biscay, North Atlantic): *Marine Geology*, v. 182, p. 279–302, doi: 10.1016/S0025-3227(01)00242-0.
- Fiske, R.S., Cashman, K.V., Shibata, A., and Watanabe, K., 1998, Tephra dispersal from Myojinsho, Japan, during its shallow submarine eruption of 1952–1953: *Bulletin of Volcanology*, v. 59, p. 262–275, doi: 10.1007/s004450050190.
- Flood, R.D., 1988, A lee wave model for deep-sea mudwave activity: *Deep-Sea Research*, v. 35, p. 973–983, doi: 10.1016/0198-0149(88)90071-4.
- Gardner, J.V., Prior, D.B., and Field, M.E., 1999, Humboldt slide—A large shear-dominated retrogressive slope failure: *Marine Geology*, v. 154, p. 323–338, doi: 10.1016/S0025-3227(98)00121-2.
- Hand, B.M., 1974, Supercritical flow in density currents: *Journal of Sedimentary Petrology*, v. 44, p. 637–648.
- Hayes, K., Montgomery, D.R., and Newhall, C.G., 2002, Fluvial sediment transport and deposition following the 1991 eruption of Mount Pinatubo: *Geomorphology*, v. 45, p. 211–224, doi: 10.1016/S0169-555X(01)00155-6.
- Hill, J.C., Driscoll, N., Weissel, J.K., and Goff, J.A., 2004, Large-scale elongated gas blowouts along the U.S. continental margin: *Journal of Geophysical Research*, v. 109, p. B09101, doi: 10.1029/2004JB002969.
- Howe, J.A., 1996, Turbidite and contourite sediment waves in the northern Rockall Trough: North Atlantic Ocean: *Sedimentology*, v. 43, p. 219–234.
- Jerolmack, D., and Mohrig, D., 2005a, Interactions between bed forms: Topography, turbulence, and transport: *Journal of Geophysical Research*, v. 110, p. F02014, doi: 10.1029/2004JF000126.
- Jerolmack, D.J., and Mohrig, D., 2005b, A unified model for subaqueous bed form dynamics: *Water Resources Research*, v. 41, p. W12421, doi: 10.1029/2005WR004329.
- Johnson, R.W., 1979, Geotectonics and volcanism in Papua New Guinea: A review of the late Cainozoic: *Bureau of Mineral Resources, Journal of Australian Geology and Geophysics*, v. 4, p. 181–207.
- Johnson, R.W., 1987, Large-scale volcanic cone collapse: The 1888 slope failure of Ritter volcano, and other examples from Papua New Guinea: *Bulletin of Volcanology*, v. 49, p. 669–679, doi: 10.1007/BF01080358.
- Kidd, R.B., Lucchi, R.G., Gee, M., and Woodside, J.M., 1998, Sedimentary processes in the Stromboli Canyon and the Marsili Basin, SE Tyrrenian Sea: Results from sidescan sonar surveys: *Geo-Marine Letters*, v. 18, p. 146–154, doi: 10.1007/s003670050062.
- Kneller, B., and Buckee, C., 2000, The structure and fluid mechanics of turbidity currents: A review of some recent studies and their geological implications: *Sedimentology*, v. 47, p. 62–94, doi: 10.1046/j.1365-3091.2000.04731062.x.
- Kubo, Y., and Nakajima, T., 2002, Laboratory experiments and numerical simulations of sediment-wave formation by turbidity currents: *Marine Geology*, v. 192, p. 105–121, doi: 10.1016/S0025-3227(02)00551-0.
- Lee, H.J., Syvitski, J.P.M., Parker, G., Orange, D., Locat, J., Hutton, E.W.H., and Imran, J., 2002, Distinguishing sediment waves from slope failure deposits: Field examples, including the ‘Humboldt slide,’ and modeling results: *Marine Geology*, v. 192, p. 79–104, doi: 10.1016/S0025-3227(02)00550-9.
- Lee, S.E., Talling, P.J., Ernst, G.G.J., and Hogg, A.J., 2002, Occurrence and origin of submarine plunge pools at the base of the US continental slope: *Marine Geology*, v. 185, p. 363–377, doi: 10.1016/S0025-3227(01)00298-5.
- Lee, S.H., and Chough, S.K., 2001, High-resolution (2–7 kHz) acoustic and geometric characters of submarine creep deposits in the South Korea Plateau: East Sea: *Sedimentology*, v. 48, p. 629–644, doi: 10.1046/j.1365-3091.2001.00383.x.
- Lewis, K.B., and Pantin, H.M., 2002, Channel-axis, overbank and drift sediment waves in the southern Hikurangi Trough, New Zealand: *Marine Geology*, v. 192, p. 123–151, doi: 10.1016/S0025-3227(02)00552-2.

- Lowe, D.R., 1982, Sediment gravity flows. II. Depositional models with special reference to the deposits of high-density turbidity currents: *Journal of Sedimentary Petrology*, v. 52, p. 279–297.
- Madsen, J.A., and Lindley, I.D., 1994, Large-scale structures on Gazelle Peninsula, New Britain: Implications for the evolution of the New Britain Arc: *Australian Journal of Earth Sciences*, v. 41, p. 561–569.
- Marr, J.G., Harff, P.A., Shanmugam, G., and Parker, G., 2001, Experiments on subaqueous sandy gravity flows: The role of clay and water content in flow dynamics and depositional structures: *Geological Society of America Bulletin*, v. 113, p. 1377–1386, doi: 10.1130/0016-7606(2001)113<1377:EOSSGF>2.0.CO;2.
- McAlpine, J.R., and Keig, G., 1983, Climate of Papua New Guinea: Canberra, Australian National University Press, 200 p.
- Middleton, G.V., 1993, Sediment deposition from turbidity currents: Annual Review of Earth and Planetary Sciences, v. 21, p. 89–114, doi: 10.1146/annurev.ca.21.050193.000513.
- Middleton, G.V., and Hampton, M.A., 1976, Subaqueous sediment transport and deposition by sediment gravity flows, in Stanley, D.J., and Swift, D.J.P., eds., *Marine Sediment Transport and Environmental Management*: New York, Wiley, p. 197–218.
- Migeon, S., Savoie, B., Zanella, E., Mulder, T., Faugères, J.-C., and Weber, O., 2001, Detailed seismic-reflection and sedimentary study of turbidite sediment waves on the Var Sedimentary Ridge (SE France): Significance for sediment transport and deposition and for the mechanisms of sediment-wave construction: *Marine and Petroleum Geology*, v. 18, p. 179–208, doi: 10.1016/S0264-8172(00)00060-X.
- Milliman, J.D., 1995, Sediment discharge to the ocean from small mountainous rivers: The New Guinea example: *Geo-Marine Letters*, v. 15, p. 127–133, doi: 10.1007/BF01204453.
- Milliman, J.D., and Syvitski, J.P.M., 1992, Geomorphic/tectonic control of sediment discharge to the ocean: The importance of small mountain rivers: *Journal of Geology*, v. 100, p. 525–544.
- Mohrig, D., and Smith, J.D., 1996, Predicting the migration rates of subaqueous dunes: *Water Resources Research*, v. 32, p. 3207–3217, doi: 10.1029/96WR01129.
- Mulder, T., and Alexander, J., 2001, The physical character of subaqueous sediment density flows and their deposits: *Sedimentology*, v. 48, p. 269–299, doi: 10.1046/j.1365-3091.2001.00360.x.
- Mulder, T., and Syvitski, J.P.M., 1995, Turbidity currents generated at river mouths during exceptional discharges to the world oceans: *Journal of Geology*, v. 103, p. 285–299.
- Mulder, T., Syvitski, J.P.M., and Skene, K.I., 1998, Modeling of erosion and deposition by turbidity currents generated at river mouths: *Journal of Sedimentary Research*, v. 68, p. 124–137.
- Mulder, T., Migeon, S., Savoie, B., and Faugères, J.-C., 2001, Inversely graded turbidite sequences in the deep Mediterranean: A record of deposits from flood-generated turbidity currents?: *Geo-Marine Letters*, v. 21, p. 86–93, doi: 10.1007/s003670100071.
- Mulder, T., Migeon, S., Savoie, B., and Faugères, J.-C., 2002, Reply to discussion by Shanmugam on Mulder et al. (2001, *Geo-Marine Letters*, v. 21, p. 86–93), Inversely graded turbidite sequences in the deep Mediterranean: A record of deposits from flood-generated turbidity currents?: *Geo-Marine Letters*, v. 22, p. 112–120, doi: 10.1007/s00367-002-0096-8.
- Mulder, T., Syvitski, J.P.M., Migeon, S., Faugères, J.-C., and Savoie, B., 2003, Marine hyperpycnal flows: Initiation, behavior, and related deposits. A review: *Marine and Petroleum Geology*, v. 20, p. 861–882, doi: 10.1016/j.marpetgeo.2003.01.003.
- Nakajima, T., and Satoh, M., 2001, The formation of large mudwaves by turbidity currents on the levees of the Toyama deep-sea channel, Japan Sea: *Sedimentology*, v. 48, p. 435–463, doi: 10.1046/j.1365-3091.2001.00373.x.
- Normark, W.R., Hess, G.R., Stow, D.A.V., and Bowen, A.J., 1980, Sediment waves on the Monterey Fan levee: A preliminary physical interpretation: *Marine Geology*, v. 37, p. 1–18, doi: 10.1016/0025-3227(80)90009-2.
- O’Leary, D.W., and Laine, E., 1996, Proposed criteria for recognizing intrastratal deformation features in marine high resolution seismic reflection profiles: *Geo-Marine Letters*, v. 16, p. 305–312, doi: 10.1007/BF01245561.
- Parsons, J.D., Bush, J.W.M., and Syvitski, J.P.M., 2001, Hyperpycnal plume formation from riverine outflows with small sediment concentrations: *Sedimentology*, v. 48, p. 465–478, doi: 10.1046/j.1365-3091.2001.00384.x.
- Pickup, G., 1984, Geomorphology of tropical rivers: I. Landforms, hydrology, and sedimentation in the Fly and lower Purari, Papua New Guinea, in Schick, A.P., ed., *Channel Processes—Water, Sediment, Catchment Controls*: Braunschweig, Catena Supplement 5, p. 1–17.
- Pigram, C.J., and Davies, H.L., 1987, Terranes and the accretion history of the New Guinea orogen: Bureau of Mineral Resources, *Journal of Australian Geology and Geophysics*, v. 10, p. 193–211.
- Schwehr, K., Driscoll, N., Tauxe, L., 2007, Origin of continental margin morphology; submarine-slide or downslope current-controlled bedforms, a rock magnetic approach: *Marine Geology*, v. 240, p. 19–41.
- Scully, M.E., Friedrichs, C.T., and Wright, L.D., 2002, Application of an analytical model of critically stratified gravity-driven sediment transport and deposition to observations from the Eel River continental shelf, Northern California: *Continental Shelf Research*, v. 22, p. 1951–1974, doi: 10.1016/S0278-4343(02)00047-X.
- Shanmugam, G., 2000, 50 years of the turbidite paradigm (1950s–1990s): Deep-water processes and facies models—A critical perspective: *Marine and Petroleum Geology*, v. 17, p. 285–342, doi: 10.1016/S0264-8172(99)00011-2.
- Shanmugam, G., 2002, Discussion on Mulder et al. (2001, *Geo-Marine Letters*, v. 21, p. 86–93), Inversely graded turbidite sequences in the deep Mediterranean: A record of deposits from flood-generated turbidity currents?: *Geo-Marine Letters*, v. 22, p. 108–111, doi: 10.1007/s00367-002-0100-3.
- Skene, K.I., Mulder, T., and Syvitski, J.P.M., 1997, INFLO1: A model predicting the behaviour of turbidity currents generated at river mouths: *Computers & Geosciences*, v. 23, p. 975–991, doi: 10.1016/S0098-3004(97)00064-2.
- Sommerfield, C.K., and Nittrouer, C.A., 1999, Modern accumulation rates and a sediment budget for the Eel shelf: A flood-dominated depositional environment: *Marine Geology*, v. 154, p. 227–241, doi: 10.1016/S0025-3227(98)00115-7.
- Stow, D.A.V., Reading, H.G., and Collinson, J.D., 1996, Deep seas, in Reading, H.G., ed., *Sedimentary Environments: Processes, Facies, and Stratigraphy*: Oxford, UK, Blackwell Science, p. 395–453.
- Taylor, B., 1979, Bismarck Sea: Evolution of a backarc basin: *Geology*, v. 7, p. 171–174, doi: 10.1130/0091-7613(1979)7<171:BSEOB>2.0.CO;2.
- Walsh, J.P., and Nittrouer, C.A., 2003, Contrasting styles of off-shelf sediment accumulation in New Guinea: *Marine Geology*, v. 196, p. 105–125, doi: 10.1016/S0025-3227(03)00069-0.
- Ward, S.N., 2001, Landslide tsunami: *Journal of Geophysical Research*, v. 106, p. 11,201–11,215, doi: 10.1029/2000JB900450.
- Warrick, J.A., and Milliman, J.D., 2003, Hyperpycnal sediment discharge from semiarid southern California rivers: Implications for coastal sediment budgets: *Geology*, v. 31, p. 781–784, doi: 10.1130/G19671.1.
- Wynn, R.B., and Stow, D.A.V., 2002, Classification and characterization of deep-water sediment waves: *Marine Geology*, v. 192, p. 7–22, doi: 10.1016/S0025-3227(02)00547-9.
- Wynn, R.B., Masson, D.G., Stow, D.A.V., and Weaver, P.P.E., 2000, Turbidity current sediment waves on the submarine slopes of the western Canary Islands: *Marine Geology*, v. 163, p. 185–198, doi: 10.1016/S0025-3227(99)00101-2.

MANUSCRIPT ACCEPTED BY THE SOCIETY 24 APRIL 2007

## Geological Society of America Special Papers

### Sediment waves in the Bismarck Volcanic Arc, Papua New Guinea

Gary Hoffmann, Eli Silver, Simon Day, et al.

*Geological Society of America Special Papers* 2008;436; 91-126  
doi:10.1130/2008.2436(05)

---

**E-mail alerting services** click [www.gsapubs.org/cgi/alerts](http://www.gsapubs.org/cgi/alerts) to receive free e-mail alerts when new articles cite this article

**Subscribe** click [www.gsapubs.org/subscriptions](http://www.gsapubs.org/subscriptions) to subscribe to Geological Society of America Special Papers

**Permission request** click [www.geosociety.org/pubs/copyrt.htm#gsa](http://www.geosociety.org/pubs/copyrt.htm#gsa) to contact GSA.

Copyright not claimed on content prepared wholly by U.S. government employees within scope of their employment. Individual scientists are hereby granted permission, without fees or further requests to GSA, to use a single figure, a single table, and/or a brief paragraph of text in subsequent works and to make unlimited copies of items in GSA's journals for noncommercial use in classrooms to further education and science. This file may not be posted to any Web site, but authors may post the abstracts only of their articles on their own or their organization's Web site providing the posting includes a reference to the article's full citation. GSA provides this and other forums for the presentation of diverse opinions and positions by scientists worldwide, regardless of their race, citizenship, gender, religion, or political viewpoint. Opinions presented in this publication do not reflect official positions of the Society.

---

Notes

---

Geological Society of America

